Cement and Concrete Research 162 (2022) 106984

Contents lists available at ScienceDirect

Cement and Concrete Research

journal homepage: www.elsevier.com/locate/cemconres

Durability of alkali-activated Fe-rich fayalite slag-based mortars subjected to different environmental conditions

Adeolu Adediran [a,*], Juho Yliniemi [a], Valter Carvelli [b], Elijah Adesanya [a], Mirja Illikainen [a]

[a] Fibre and Particle Engineering Research Unit, University of Oulu, Pentti Kaiteran katu 1, 90014 Oulu, Finland
[b] Department A.B.C., Politecnico di Milano, Piazza Leonardo Da Vinci 32, 20133 Milan, Italy

ARTICLE INFO

Keywords:
Fe-rich fayalite slag
Ladle slag
Blast furnace slag
Alkali activated materials
Durability

ABSTRACT

Fe-rich alkali activated materials (AAMs) require detailed understanding of their durability prior to their real-life application in the construction industry. Three mixes were formulated with fayalite slag (FS) as the main precursor. The effect of incorporation of ladle slag (LS) or blast furnace slag (BFS) on the shrinkage and exposure to physical and chemical attacks representing environmental conditions in cold and tropical regions (acidic solution at room temperature and in freeze-thaw, combined sodium sulfate and sodium chloride solution at room temperature and in freeze-thaw, freeze-thaw in water and dry-wet cycles) was investigated via visual observation, mass loss, compressive strength, X-ray diffraction (XRD), mercury intrusion porosimetry (MIP), and scanning electron microscope coupled with energy dispersive X-ray spectroscopy (SEM-EDS). Experimental results show the considerable role of incorporated LS and BFS in modifying the gels formed and controlling material degradation of blended AAMs after exposure. In contrast, sole FS-based samples were completely degraded particularly those exposed to freeze-thaw in water, acid, and combined sodium sulfate and sodium chloride solution, indicating their vulnerability to frost and chemical attacks.

1. Introduction

Properly designed concrete made with Portland cement (PC) can be durable when exposed to normal environment [1,2]. However, it has been observed that PC-based concrete can deteriorate or degrade when exposed to severe and aggressive conditions [3]. The exposure to these conditions may lead to increased porosity, spalling, cracking and loss of strength, which shortens the service life and increases the maintenance requirements of the concrete [4]. Hence, there is increasing demand for alternative binders that can perform under diverse chemical and environmental stresses.

The durability properties of alkali-activated materials (AAMs) or geopolymers exposed to different environmental conditions have been widely studied in the literature using several precursors such as blast furnace slags (BFS), fly ash (FA), and metakaolin to replace PC-based concrete [5–10]. Compared to conventional PC concrete which contain calcium silicate hydrate as the main phase, the reaction products formed in AAMs is quite different and are mostly aluminium substituted calcium silicate hydrate (i.e. C-A-S-H) or sodium aluminium silicate hydrate (N-A-S-H) depending on the type of precursor [2]. Meanwhile, AAMs has shown better resistance when subjected to physical and chemically induced deterioration such as acid attacks [11,12], freeze and thaw [13], wetting and drying [14,15], chloride penetration [16], carbonation [17] and corrosion [18]. While significant amount of research has been carried out on the durability of AAMs based on FA, BFS and ferronickel slags [19–21], the durability of AAMs based on fayalite slags (FS) exposed to different environmental conditions is not fully understood and therefore needs to be investigated.

Fayalite slag is one of the most common Fe-rich industrial residues emanating from copper and nickel production, which are mostly disposed to landfills or used in low value applications, resulting in higher landfilling costs for the production companies [22]. Over the years, the production of FS has continued to rise with the increasing demand for copper and nickel for varied applications and approximately 200,000 tons of water-quenched nickel slag and 400,000 tons of slowly-cooled copper slag are generated annually in Finland [23]. The amount of FS disposed annually is enormous and this provides a solid reason to thoroughly investigate and find alternative pathway and technologies that could facilitate the reuse of this industrial residue.

The mineralogical and chemical composition of FS mostly depends on the ore source and composition, processing operations and cooling process, but usually consists of Fe_2O_3 and SiO_2 with lower amount of

* Corresponding author.
E-mail address: adeolu.adediran@oulu.fi (A. Adediran).

https://doi.org/10.1016/j.cemconres.2022.106984
Received 17 June 2022; Received in revised form 26 August 2022; Accepted 12 September 2022

Table 1
Chemical composition (wt%), LOI, density and particle size distribution of FS, BFS and LS.

	FS	BFS	LS
SiO_2	34.4	32.3	9.3
Al_2O_3	2.4	9.58	29.6
Fe_2O_3	52.5	1.23	1.8
CaO	1.9	38.5	48.6
MgO	6.8	10.2	6.6
Na_2O	0.5	0.5	0.2
K_2O	0.6	0.5	0.03
TiO_2	0.2	2.2	1.5
P_2O_5	0.04	0.0	0.03
MnO	0.08	0.0	0.9
SO_3	0.5	4.0	0.4
LOI at 950 °C	−0.2	0.5	1.3
LOI at 525 °C		–	–
Density (g/cm^3)	3.8	2.9	3.0
d_{10} [μm]	0.7	0.6	1.3
d_{50} [μm]	9.3	10.1	9.6
d_{90} [μm]	44.4	76.8	45.3

Table 2
Mineralogy and phase composition of the precursors.

Phases	Formula	LS	FS	BFS
Mayenite	$C_{12}A_7$	30.9	–	
Calcio-olivine	γ - C_2S	21.3	–	
Tricalcium-aluminate	C_3A	12.9	–	
Q- phase	$Ca_{20}Al_{26}Mg_3Si_3O_{68}$	14.4	–	
Periclase	MgO	8.2	–	
Perovskite	$CaTiO_3$	1.3	–	
Fayalite	Fe_2SiO_4	–	43.1	
Magnetite	Fe_3O_4	–	1.6	
Amorphous		11	55.3	100

Al_2O_3 and CaO [22,24]. Due to its physico-chemical properties, FS has been previously adopted as sand replacement, road construction, pozzolanic material with PC, sandblasting and filler material [25]. Meanwhile, the recent needs to cut down the CO_2 emissions associated with cement production and excessive consumption of known precursors such as BFS and FA, either as supplementary cementitious materials for cement production or as precursors for AAMs, has prompted the identification and reuse of FS as precursors for AAMs [26]. Because FS contains some amorphous content due to water granulation during the cooling process, FS is reactive when exposed to alkaline environment [27,28]. The amorphous phase of FS is structurally disordered which makes it more prone to dissolution in alkali activating solution, releasing constituents such as Fe, Si, Mg into the solution as monomers [29,30]. The formation of oligomers takes place once some saturation level or certain concentration of species in the solution is reached which cross-link into polymers prior to the formation of the binder gel [31]. However, when cured at ambient temperature, alkali-activated FS provides weak cross-link network of polymers due to relatively high concentration of Fe and lower Ca and Al content, resulting in lower reactivity and mechanical performance compared to other aluminosilicates such as BFS and LS [32].

To overcome the low inherent reactivity of FS and achieve good properties at ambient temperature, several approaches have been investigated and reported in literatures with promising results [22,27,28,33–35]. For instance, in a recent study of the authors, the synergistic blend of FS with other highly reactive precursors such as LS and BFS, mixed with an alkaline solution, was beneficial for its overall performance at ambient temperature (Unpublished). However, most of the studies conducted so far on the utilization of FS as precursors for AAMs and blended cements have focused on the reactivity, mechanical, microstructure and structural properties with limited study on their stability when exposed to different aggressive environmental conditions. This makes the practical application of FS limited, due to some uncertainties regarding the durability in different aspects such as: freeze-thaw resistance, combined sulfate and chloride resistance, acid resistance and dry-wet resistance. Moreover, due to difference in mineralogical composition, chemical composition, reaction mechanisms and product composition of FS compared to other widely used precursors, the durability properties of alkali-activated FS may vary and therefore needs to be thoroughly investigated to facilitate their use for construction applications. Furthermore, since FS has been identified as an Fe-rich silicate, but Ca and Al-deficient material, LS and BFS were incorporated as reactive calcium and aluminium source and their influence on the durability properties of alkali-activated FS was investigated.

To the best of the authors' knowledge, this is the first study presenting a systematic and detailed investigation on the durability properties of alkali-activated FS and alkali-activated FS composite containing LS or BFS exposed to physical attacks, chemical attacks, and combined physical and chemical attacks. The present study aims to develop highly durable alkali-activated FS materials by adding other Ca- and Al-rich precursors such as BFS and LS. The effects of LS or BFS addition on the behavior of alkali-activated FS mortars exposed to different environmental conditions that mimic the combined load from multiple chemical solutions and environmental stresses in cold climate and tropical regions (acidic solution at room temperature, acidic solution in freeze-thaw cycles, combined sodium sulfate and sodium chloride solution at room temperature, combined sodium sulfate and sodium chloride solution in freeze-thaw cycles, freeze-thaw cycles in water and dry-wet cycles) were investigated. The macro and micro effects after exposure to different environmental conditions were studied using visual observation, mass loss, compressive strength, X-ray diffraction (XRD), mercury intrusion porosimetry (MIP), and scanning electron microscope coupled with energy dispersive X-ray spectroscopy (SEM-EDS).

2. Experimental program

2.1. Precursor's characterization

Water-quenched Fe-rich FS used as starting material in this study is an industrial residue or by-product from nickel production, supplied in granular form by Boliden Harjavalta, Finland. LS used as co-binder in this experiment is an industrial residue from steel production collected from slag cooling pit of SSAB (Raahe, Finland) after exposure to natural cooling. Commercially available BFS used as another co-binder in this study was supplied by Finnsementti (Finland). Prior to the usage of FS as sole solid precursor (aggregate and binder), the as-received FS was dried in the oven at a temperature of 60 °C for 24 h to remove the residual moisture. FS was milled for 3 h using a laboratory ball mill (TPR-D-950-V-FU-EH, Germatec, Germany) with 150 optimized stainless-steel ball sizes (45 balls of Ø 40 mm, 45 balls of Ø 30 mm and 60 balls of Ø 25 mm) to achieve a median particle size (d_{50}) of 10 μm. For each milling batch, 2 kg of FS was loaded into the ball mill container and the milling was performed using a critical speed of 82 rpm. Using the same milling procedure and ball sizes, 2 kg of as-received LS was milled for 2 h to achieve similar d_{50} as milled FS. Prior to milling LS, the as-received LS was first sieved using a 2 mm mesh to remove the leftover steel flakes that might interfere with the milling process. The longer milling time needed for FS is due to its higher hardness and initial bigger particle size compared to LS and this prolongs the comminution process and consequently energy consumption and costs of milling. On the other hand, BFS was supplied in milled form and therefore used as received. The particle size distribution of FS, BFS and LS was analyzed using a laser diffraction particle size analyzer (LS 13320, Beckman Coulter, USA). For the particle size measurement, water was used as a dispersing medium for FS while isopropanol was used for LS and BFS to prevent reaction of particles with water during measurement.

Table 3
Mix design of mortar samples.

	FS (g)	BFS (g)	LS (g)	FSA (g)	SH[a] (g)	SS[b] (g)	Curing temperature (°C)
AAFS	100	0	0	200	22.5	22.5	23 ± 2 °C
AAFS-BFS	80	20	0	200	22.5	22.5	
AAFS-LS	80	0	20	200	22.5	22.5	

a - sodium hydroxide solution; b - sodium silicate solution.

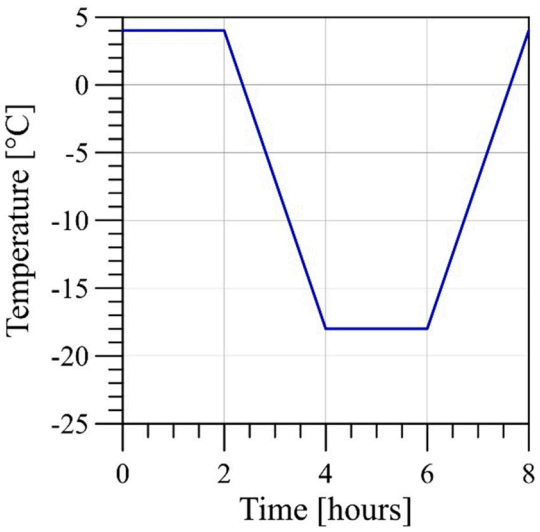

Fig. 1. Freeze-thaw test program for one cycle.

The chemical composition of FS, BFS and LS, together with their loss on ignition (LOI) was analyzed by X-ray fluorescence (XRF) (PANalytical Omnian Axiosmax, UK) at 4 kV from a melt fused tablet. The density of the materials was measured using helium pycnometer (Micrometrics, USA). Five replicate density measurements were taken, and the average regarded as the density value. The chemical composition, LOI, particle size distributions and density of materials are presented in Table 1. The mineralogical and phase composition of FS, BFS and LS are obtained by quantitative XRD, as presented in Table 2. From the table, it can be seen that the amorphous content varies among the precursors. Meanwhile, the amorphous content of FS is above 50 % and is comparable to similar slags reported in the literature [19]. The XRD procedure is described in detail in Section 2.3.5.

2.2. Mix designs, sample preparation and curing conditions

Three mix compositions were designed for this study and presented in Table 3. The reference sample denoted as AAFS was made with only FS (aggregate and binder). The remaining two mix compositions were formulated by replacing FS binder with 20 wt% of LS (named 'AAFS-LS') or BFS (named 'AAFS-BFS'). The optimal LS and BFS content addition were determined based on the results of preliminary experiments and our previous study (Unpublished results). The alkali activator used for the synthesis was a mixture of analytical grade sodium silicate solution (Merck, USA) and 10 M sodium hydroxide (NaOH) solution as suggested in [22]. The NaOH solution was prepared using analytical grade NaOH pellets (>98 % purity; VWR Chemicals, Germany) dissolved in laboratory controlled deionized water and allowed to cool down. The target activator has a final molar ratio (SiO_2/Na_2O = 1.0) and (H_2O/Na_2O = 15.7) and was prepared 24 h before mixing with the precursors. According to ref. [22], it was revealed that using granular FS (named 'FSA') in place of standard sand for mortar preparation not only encourages full recycling of FS but also improves the mechanical and microstructural properties of AAMs produced. Based on this, FSA was used as the aggregate source in the preparation of the mortars in this study and the aggregate to binder ratio was kept at 2. The mixing of the mortar samples was performed in accordance with EN 196-1 standard [36] and the workability of the fresh mortar samples was assessed using a flow table test in accordance with the EN 1015-3 standard [37]. Thereafter, the fresh mortars were cast into 50 mm × 50 mm × 50 mm and 40 mm × 40 mm × 160 mm molds and compacted using a jolting machine (60 shocks, 1/s). After compaction, the mortars in the molds were covered with plastic bags and placed at room temperature. After 24 h, the samples were then demolded, kept, and cured in a sealed plastic bag prior to durability testing and analysis.

2.3. Experimental methods overview

2.3.1. Drying shrinkage

The drying shrinkage of all the mortar samples was taken at 1, 3, 7, 21, 28, 56 and 90 days to determine the change in length. Duplicates samples cured at room temperature and relative humidity of 60 % were used. The length measured after 24 h was taken as the initial length (L_o) while L_t is the length taken at each of the days. The change in length due to drying shrinkage over time is calculated according to EN 12617-4 standard, using:

$$\Delta L = \frac{L_0 - L_t}{L_i} \times 100$$

where L_i = nominal effective length of the mold.

2.3.2. Freeze-thaw cycling and ambient aging

Freeze–thaw resistance of all the mortar samples was tested in accordance to ASTM C666/C666M-15 [38]. Three mortar samples (28 d age) for each mix were placed in three solutions namely tap water, combined sodium sulfate and sodium chloride solution and sulfuric acid solution (pH = 1) in a climate chamber (WK3-180/40, Weiss Technik, Grand Rapids, Germany). The solution level and pH were kept constant throughout the testing period and a total of 180 freeze-thaw cycles (approximately 2 months) were conducted. The temperature of one cycle was from to −18 °C to +4 °C and the duration of each cycle was 8 h. The schematic representation of one cycle program is shown in Fig. 1. Simultaneously, triplicate samples for each mix were also immersed in the same solutions mentioned above except for water and placed at room temperature for 2 months for comparison. The former was to simulate the aggressive climatic condition in the cold region, while the latter represented the aggressive condition in the tropical region. The 5 % sulfuric acid (>97 % purity; VWR Chemicals, Germany) solution was prepared according to the study in ref. [39]. Furthermore, the combination of 5 % sodium sulfate (product code 1.06649.0500 by Merck, Germany) and 3 % sodium chloride (product code 7647-14-5 by J. T. Baker, the Netherlands) solution prepared for the analysis was based on the study reported in ref. [40], mimicking aggressive marine conditions. The solutions fully covered the samples and were replaced after every 15 days (45 cycles).

2.3.3. Visual observation and mass loss

Changes in the mortar samples visual aspects such as colour change and macrocracks were observed by naked eye. Moreover, the mass variation of samples before and after exposure to these environments was calculated as in ref. [40]

$$\Delta M = \frac{M_t - M_o}{M_o} \times 100$$

where M_t is the mass of the specimen at time t (kg), and M_o is the initial mass (kg) of the specimen at the initial state (before exposure).

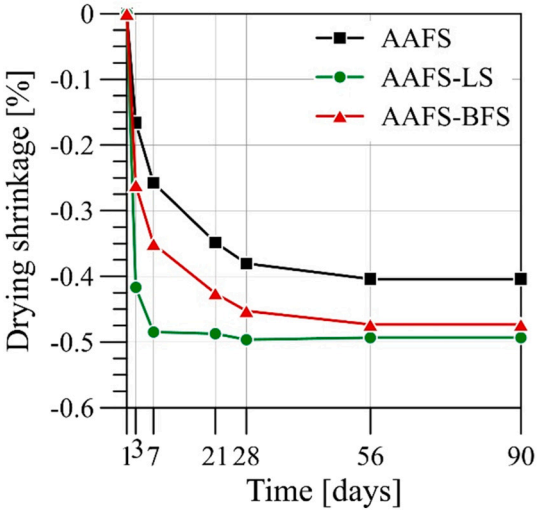

Fig. 2. Drying shrinkage of AAFS, AAFS-BFS and AAFS-LS cured in air at RH 65 % measured until 90 days.

2.3.4. *Compressive strength*

To assess the mechanical performance of the materials, the compressive strength of mortar samples before and after exposure to aggressive environment in the climatic chamber were tested at 0, 90 and 180 cycles, while those placed at room temperature were tested at 0, 30 and 60 days (three tests for each material and exposition). Also, the dry-wet strength was carried out on all the mortar samples (28 d age). The test included immersing the specimens in water for 24 h and then drying the wetted specimens for 24 h at room temperature for a duration of 2 months (60 days). After 30 and 60 days, triplicate samples of each mix were measured for their residual compressive strength.

The compressive strength of the mortar samples was measured using a Zwick testing equipment (Zwick Roell Group, Ulm, Germany) with a load cell of 100 kN and a loading rate of 2.4 kN/s.

2.3.5. *XRD analysis*

The XRD analysis of the precursors (FS, BFS and LS) and their corresponding AAMs (AAFS, AAFS-LS and AAFS-BFS) before and after exposure to aggressive environments were carried out using a Rigaku Smartlab diffractometer. The analysis utilizes Cu Kα radiation operated at 40 kV and 135 mA and a scanning rate of 0.02°2θ/step from 5 to 80°. The quantification of the crystalline phases was done with the addition of 10 wt% rutile (TiO_2) to the powdered samples as the internal standard. The quantitative X-ray diffraction analysis (QXRD) was done using PDXL2 software associated with the PDF-42015 database as reported in literature [19].

2.3.6. *Mercury intrusion porosimetry*

The pore size distribution and pore volume of the materials were measured by MIP technique using an AutoPore IV 9500 (Micromeritics, Italy) up to a maximum pressure of ca. 400 MPa. Mortar samples were dried at 50 °C for 12 h before measurements. One sample, weight 6–7 g, for each material and environmental condition was adopted. Despite the limited number of measurements, they gave a clear comparative insight into the effect of the precursors and environmental aging on the modification of porosity.

2.3.7. *SEM-EDS*

The microstructural observation of the mortar samples before and after exposure was investigated using SEM-EDS analysis (Zeiss Ultra Plus, Germany). The samples were carefully cut into pieces, casted in epoxy resin, polished using ethanol and carbon coated prior to analysis. Secondary electron images were captured using a backscattered electron detector with 15 kV acceleration voltage and a working distance of 8 mm.

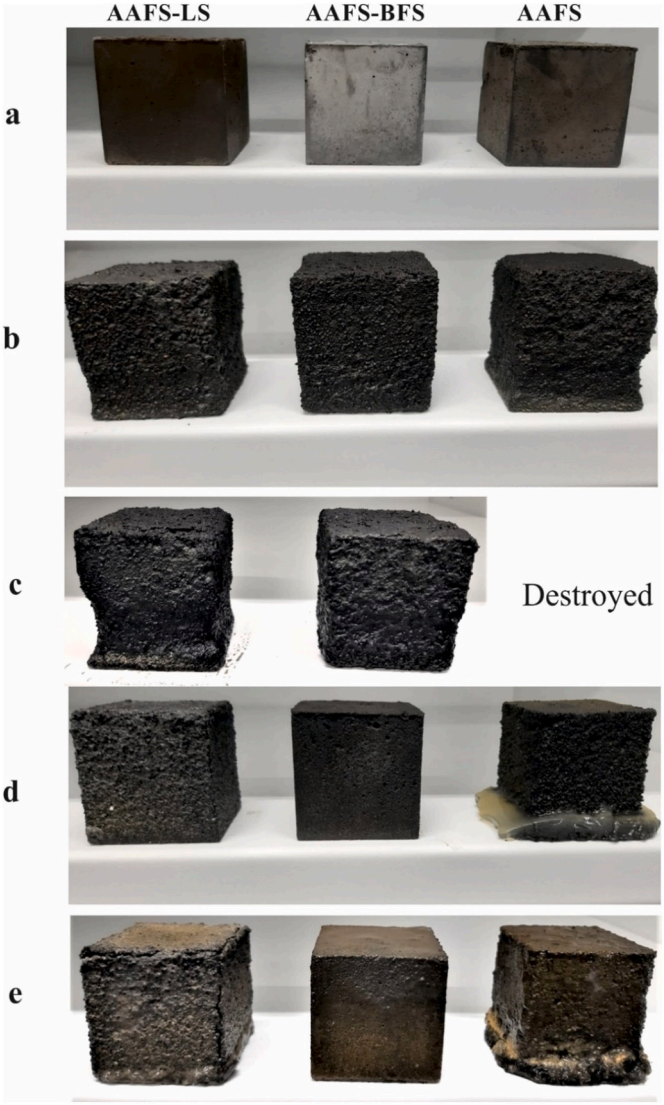

Fig. 3. Appearances of AAFS, AAFS-BFS and AAFS-LS subjected to sulfuric acid solution: (a) initial state, (b) after 90 freeze-thaw cycles in sulfuric acid solution, (c) after 180 freeze-thaw cycles in sulfuric acid solution, (d) after 30 days immersion in sulfuric acid solution at room temperature, (e) after 60 days immersion in sulfuric acid solution at room temperature. The cube dimension is 50 × 50 × 50 mm^3.

3. Results and discussion

3.1. *Drying shrinkage*

The drying shrinkage of the mortars are presented in Fig. 2. AAFS-LS has the highest drying shrinkage, followed by AAFS-BFS with the lowest drying shrinkage occurring in AAFS. Higher shrinkage values observed in blended mortars are attributed to the incorporation of LS and BFS as co-binders. Meanwhile, it was observed that the addition of LS as co-binder had more adverse effect on the shrinkage than BFS, suggesting that different co-binders has slightly different impact on the drying shrinkage. The difference in shrinkage values between AAFS-LS and AAFS-BFS is likely related to the higher Ca and Al content of LS compared to BFS, as the difference in their chemical composition can influence the reaction chemistry and responsiveness behavior of the

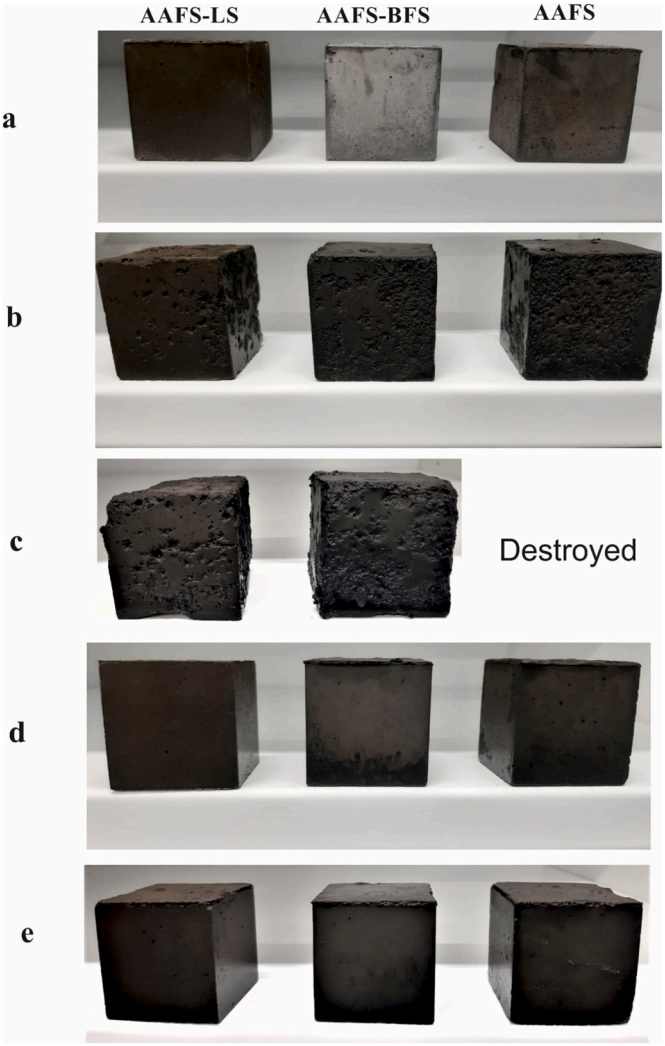

Fig. 4. Appearances of AAFS, AAFS-BFS and AAFS-LS subjected to combined sulfate and chloride solution: (a) initial state, (b) after 90 freeze-thaw cycles in combined sulfate and chloride solution, (c) after 180 freeze-thaw cycles in combined sulfate and chloride solution, (d) after 30 days immersion in combined sulfate and chloride solution at room temperature, (e) after 60 days immersion in combined sulfate and chloride solution at room temperature. The cube dimension is 50 × 50 × 50 mm^3.

blended mortars. Mastali et al. [41] reported that the drying shrinkage of AAMs is mainly influenced by the Ca/Si and Al/Si ratio. The synergetic mixture of FS with LS or BFS modified the chemical ratios of the blended mortars and is presumed to have affected the fine pore structure and consequently increase their drying shrinkage at early and late age. A refined pore structure creates a high capillary force in the material due to self-desiccation thereby causing higher shrinkage [42]. From all indications, it reflects that the pore structure of AAFS-LS and AAFS-BFS mixes got refined with addition of co-binders (see Sections 3.6 and 3.7), which results in high drying shrinkage. The high shrinkage values of the blended mortars could limit their usage in real-life applications, and thus shrinkage reducing agents or admixtures should be studied to improve this property. Higher shrinkage observed in blended mortars is consistent with those reported in the literature when BFS and other Ca-rich slags were blended with similar iron rich slags [43]. Overall, the drying shrinkage of all the samples stabilized from 56 days up to 90 days with no visible macro or micro cracks observed throughout the length change analysis.

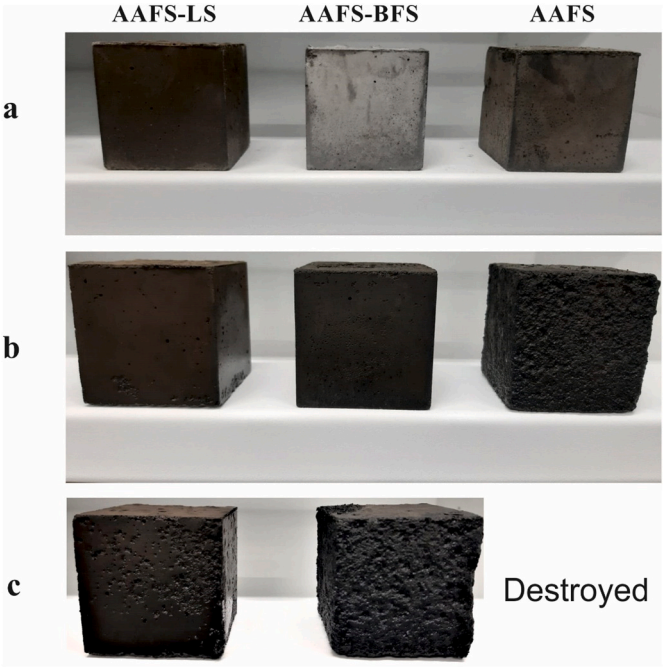

Fig. 5. Appearances of AAFS, AAFS-BFS and AAFS-LS subjected to freeze-thaw cycles in water: (a) initial state, (b) after 90 freeze-thaw cycles, (c) after 180 freeze-thaw cycles. The cube dimension is 50 × 50 × 50 mm^3.

3.2. Visual inspection

The visual appearance of all the mortar samples after exposure to different environmental conditions is presented in Figs. 3, 4, and 5. Mortar samples unexposed to these aggressive environments are also shown for comparison. Exposure to acid solution (at room temperature and under freeze-thaw conditions) caused visible damage to all the mortar samples (see Fig. 3a–e). After exposure to 90 freeze-thaw cycles in acid solution (Fig. 3b), cracks were seen around the edges of AAFS samples, with visible loss of binder from the surface leaving the aggregate completely exposed. One possible explanation could be that the weak reactivity and limited formation of reaction products, that occurred in AAFS, allows quick penetration of acid into the sample surface. As the freeze-thaw cycles increased, acid penetration and deterioration of all the samples intensified. After exposure to 180 freeze-thaw cycles in acid solution, AAFS was completely disintegrated, while blended mortars of AAFS-LS and AAFS-BFS remains stable but appears to be slightly damaged at the surface and around the edges of the samples (Fig. 3c). The stability of the blended mortars highlights the role of co-binders in terms of resisting the expansion caused by freeze-thaw process and also the chemical attacks of the acid solution. For samples placed in acid solution at room temperature, the rate of deterioration was quite low compared to those subjected to freeze-thaw conditions. After 30 days of immersion in acid solution at room temperature (Fig. 3d), a light-yellow crystal can be found at the bottom of the exposed specimen of AAFS. As the exposure time increased to 60 days, light yellow crystals appeared in all the samples and the deterioration becomes severe, with the evidence more visible in AAFS-LS and AAFS (Fig. 3e). The appearance of the light-yellow crystals may likely be attributed to the reaction between the gel and the sulfuric acid. Similar crystal formation has also been reported for volcanic ash-based geopolymer, attributed to the precipitation reaction between geopolymer gel and sulfuric acid [44]. In general, AAFS mortar samples suffered significant damage during exposure to acid solution at room temperature and in freeze-thaw environment when compared to blended mortar samples (AAFS-LS and AAFS-BFS), i.e., aggregate particles were visibly exposed due to the loss of paste from the sample surface caused by the

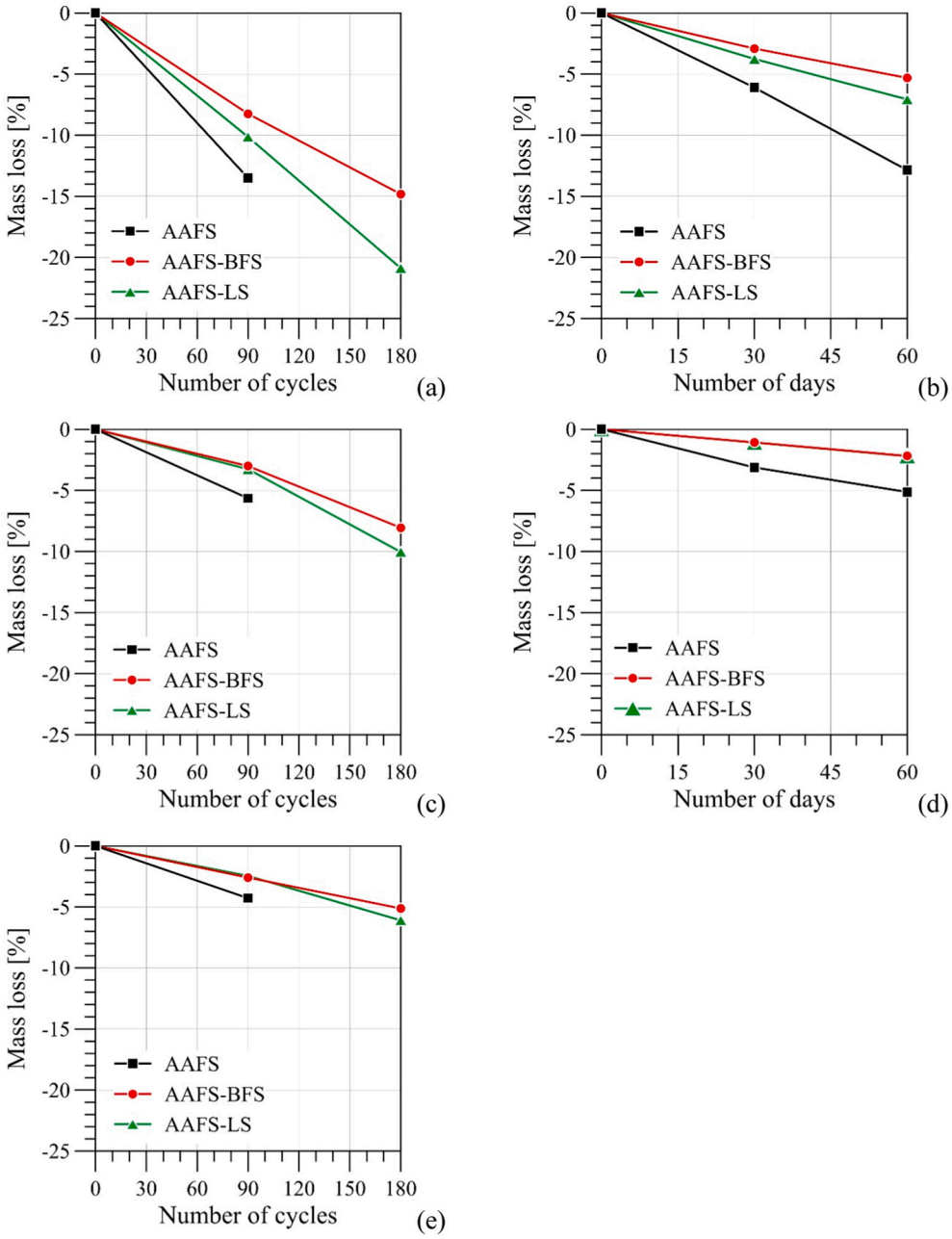

Fig. 6. Mass loss of AAFS, AAFS-BFS and AAFS-LS subjected to different aggressive environments: (a) after 90 and 180 freeze-thaw cycles in acid solution, (b) after 30- and 60-days immersion in acid solution at room temperature, (c) after 90 and 180 freeze-thaw cycles in combined sodium sulfate and chloride solution, (d) after 30- and 60-days immersion in combined sodium sulfate and chloride solution at room temperature, (e) after 90 and 180 freeze-thaw cycles in water. The error of the measurements is in the range of 0–0.5 %.

ingress of acid.

The influence of combined sulfate and chloride solution on the physical appearance of mortar samples when placed at room temperature and subjected to freeze-thaw conditions are presented in Fig. 4. The positive effects of co-binder addition on blended samples in freeze-thaw environments is confirmed by visual observation as there were no significant macro cracks observed in AAFS-LS and AAFS-BFS samples after 90 cycles in combined sulfate and chloride solution (Fig. 4b). However, partial deformation was found in AAFS-LS and AAFS-BFS samples after 180 freeze-thaw cycles (Fig. 4c). In contrast, AAFS exhibited poor freeze-thaw resistance in combined sulfate and chloride solution and was completely destroyed after 180 cycles. The significant damage observed in AAFS may likely be attributed to volume expansion of absorbed solution in the pores due to the dual effect of freeze-thaw and combined sulfate and chloride attack. On the other hand, the effect of combined sulfate and chloride solution on all the mortar samples placed at room temperature was less severe when compared to those subjected to freeze-thaw conditions. After 30 and 60 days of exposure to combined sulfate and chloride solution at room temperature, no significant damage was observed on all the mortar samples as they conserved their shape (Fig. 4d and e).

Furthermore, samples subjected to freeze-thaw cycles in water was also evaluated by visual observation and presented in Fig. 5. After 90 freeze-thaw cycles in water, AAFS-LS and AAFS-BFS samples showed no significant deterioration, but AAFS showed slightly visible damage on the outer surface (Fig. 5b). At the end of 180 cycles, AAFS-LS and AAFS-BFS was relatively stable while AAFS was completely deteriorated, indicating that AAFS is less suitable for use as sole AAMs in cold areas (Fig. 5c). Overall, the visual observation of all the samples before and after exposure to different environmental conditions indicated that the incorporation of co-binders improves the stability and provides more resistance to physical, chemical, and combined physical and chemical attacks.

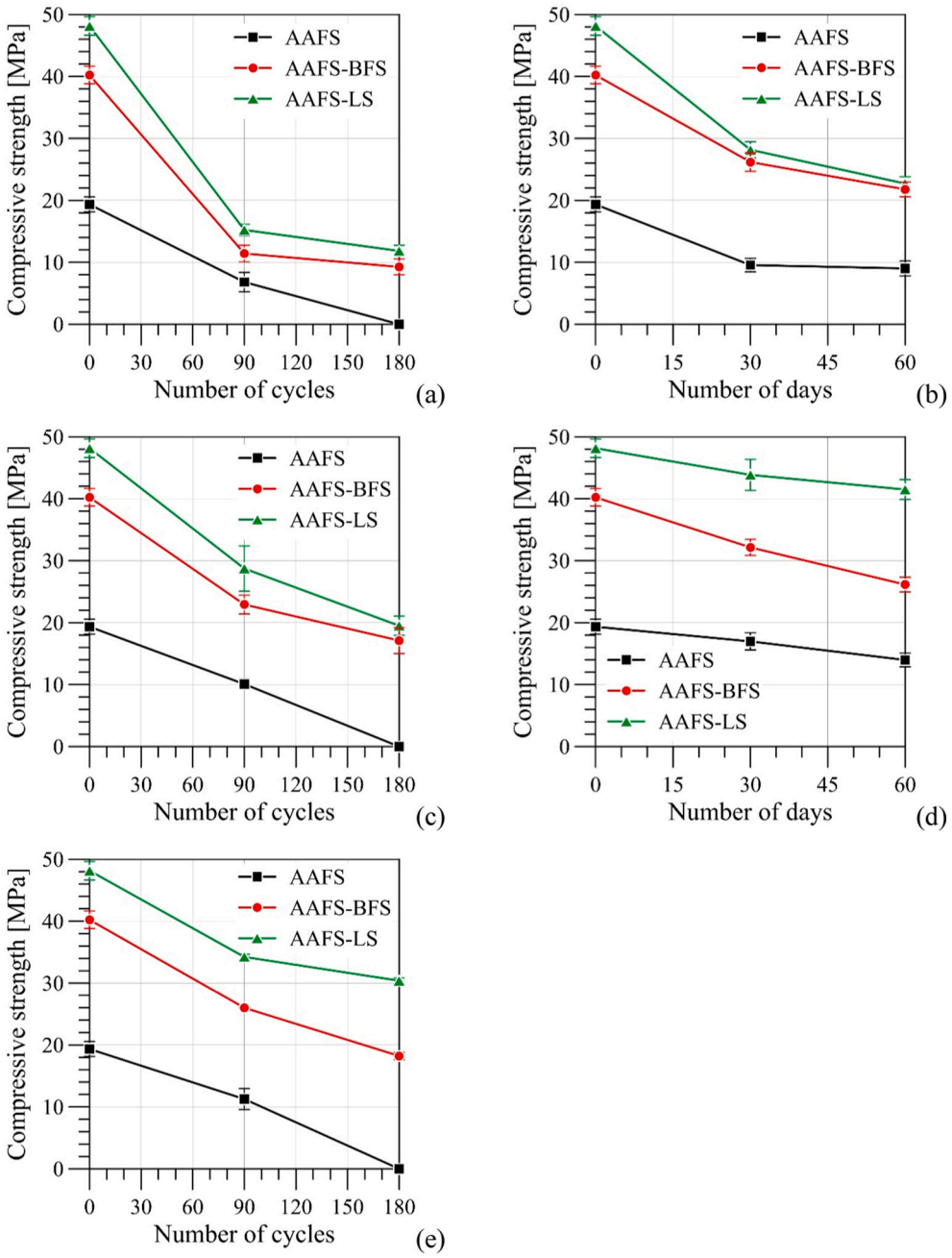

Fig. 7. Compressive strength of AAFS, AAFS-BFS and AAFS-LS subjected to different aggressive environments: (a) after freeze-thaw cycles in sulfuric acid solution, (b) after immersion in sulfuric acid solution at room temperature, (c) after freeze-thaw cycles in combined sodium sulfate and chloride solution, (d) after immersion in combined sodium sulfate and chloride solution at room temperature, (e) after freeze-thaw cycles in water. (Error bars show standard deviation of three measurements).

3.3. Mass loss

Fig. 6(a–e) shows the relationship between mass loss before and after exposure to different environmental conditions and the exposure time. The mass loss of the samples increased gradually with the increase in exposure period. After exposure to 180 freeze-thaw cycles in sulfuric acid solution, the mass loss of AAFS-LS and AAFS-BFS was 20 % and 15 %, respectively, while the mass loss of AAFS could not be measured due to complete disintegration (i.e., 100 % mass loss). The combination of freeze-thaw conditions and sulfuric acid concentration is presumed to have caused significant damage to AAFS mortars. Compared to mortars subjected to freeze-thaw conditions in sulfuric acid solution, the mass loss of alkali-activated mortar samples immersed in acid solution and placed at room temperature were much lower (Fig. 6b). After 60 days of immersion in acid solution at room temperature, AAFS-LS and AAFS-BFS lost only 7.1 % and 5.3 %, respectively, while AAFS lost 13 % of their mass (Fig. 6b). This lower mass loss rate observed in samples immersed in acid solution at room temperature is consistent with the visual observation in Fig. 3, which showed that sample immersed in acid solution at room temperature has lower deterioration level than those subjected to freeze-thaw cycles in sulfuric acid solution. Generally, mass loss of geopolymers in acid environment could be ascribed to the exchange of cations in the structure by protons and physical deterioration resulting in the detachment of some components from the sample surface [11]. Meanwhile in all the different environments (freeze-thaw and room temperature) studied during exposure to sulfuric acid solution, AAFS-LS and AAFS-BFS exhibited a lower mass loss than AAFS mortars. The lower mass loss observed in blended mortars could be ascribed to the different reaction products formed due to the incorporation of LS and BFS, which provided higher mitigating capacity for internal damage, justifying the better resistance to acid solution at room temperature and freeze-thaw conditions compared to AAFS. The observed mass losses

Table 4
Compressive strength of AAFS, AAFS-BFS and AAFS-LS during wet and dry conditions.

Sample name	Initial compressive strength (MPa)	Dry-wet compressive strength (MPa) after 30 days	Dry-wet compressive strength (MPa) after 60 days
AAFS	19	17	15
AAFS-BFS	40	38	36
AAFS-LS	48	46	43

obtained in this study are lower than those reported for PC-based concrete but agree with earlier published results on the acid resistance of alkali- activated slag/fly ash blend and other low-Ca alkali activated materials [45].

On the other hand, the results of mass loss of mortar samples subjected to combined sulfate and chloride solution at room temperature and freeze-thaw conditions are shown in Fig. 6c–d. The mass loss in all the samples after exposure is presumed to have been caused by the leaching of alkaline ion and other unreacted elements not embedded in the matrix. At both room temperature and freeze-thaw conditions, AAFS-LS and AAFS-BFS gave better resistance to combined sulfate and chloride attack, likely attributed to the inclusion of co-binders which provided a dense and more compact structure and reduced the penetrability of the solution. After 180 freeze-thaw cycles in combined sulfate and chloride solution, AAFS was completely destroyed and the mass loss of AAFS-LS and AAFS-BFS were 10 % and 8 %, respectively. For samples immersed in combined sulfate and chloride solution at room temperature, the mass loss of AAFS-LS, AAFS-BFS and AAFS was 2.2 %, 2.2 % and 5.1 %, respectively, after 60 days of exposure. The mass loss observed in this study is considerably lower than those reported for PC-based materials; the reason may likely be due to difference in reaction products between PC-based materials and AAMs which makes the mortars less susceptible to sulfate attack [46].

Furthermore, exposure to 180 freeze-thaw cycles in water resulted in the mass loss of 6.1 % and 5.1 % for AAFS-LS and AAFS-BFS respectively while AAFS was completely damaged, suggesting that blended mortars were considerably resistant to frost exposure and can be used as outdoor material in cold regions (Fig. 6e).

3.4. Compressive strength

The residual compressive strength of the mortars after exposure to aggressive environment are shown in Fig. 7a–e. Before exposure, the initial average compressive strengths of the mortar samples of AAFS, AAFS-BFS and AAFS-LS after 28 days of curing at room temperature were 19, 40, and 48 MPa, respectively. The lower initial strength exhibited by AAFS is primarily associated with low reactivity and less formation of reaction products (later discussed in Section 3.7). On the other hand, the addition of BFS and LS increased the reactive Ca and Al ion in the matrix and modified the gels formed, which lowers the porosity (see Section 3.6) and contributed to the initial higher compressive strength in AAFS-BFS and AAFS-LS. After exposure to the different environmental conditions, the compressive strength of all the samples decreased with an increase in the exposure period. It is worth mentioning that the reduction in compressive strength during exposure to sulfuric acid is generally ascribed to the breakdown of the binder and the effect of this reaction is likely to continue as long as sample is exposed to acidic medium [47]. Exposure to strong acid such as sulfuric acid can cause depolymerization of the aluminosilicate gel and breakage of Si-O-Al bonds, resulting in the deterioration of mortar which also can affect the mechanical properties of the material [11]. For instance, the compressive strength of AAFS-BFS and AAFS-LS samples after exposure to 180 freeze-thaw cycles in sulfuric acid solution decreased to 9.3 and 12 MPa, respectively, while that of AAFS could not be measured due to severe damage (Fig. 7a). As reported in the literature, freeze-thaw cycles

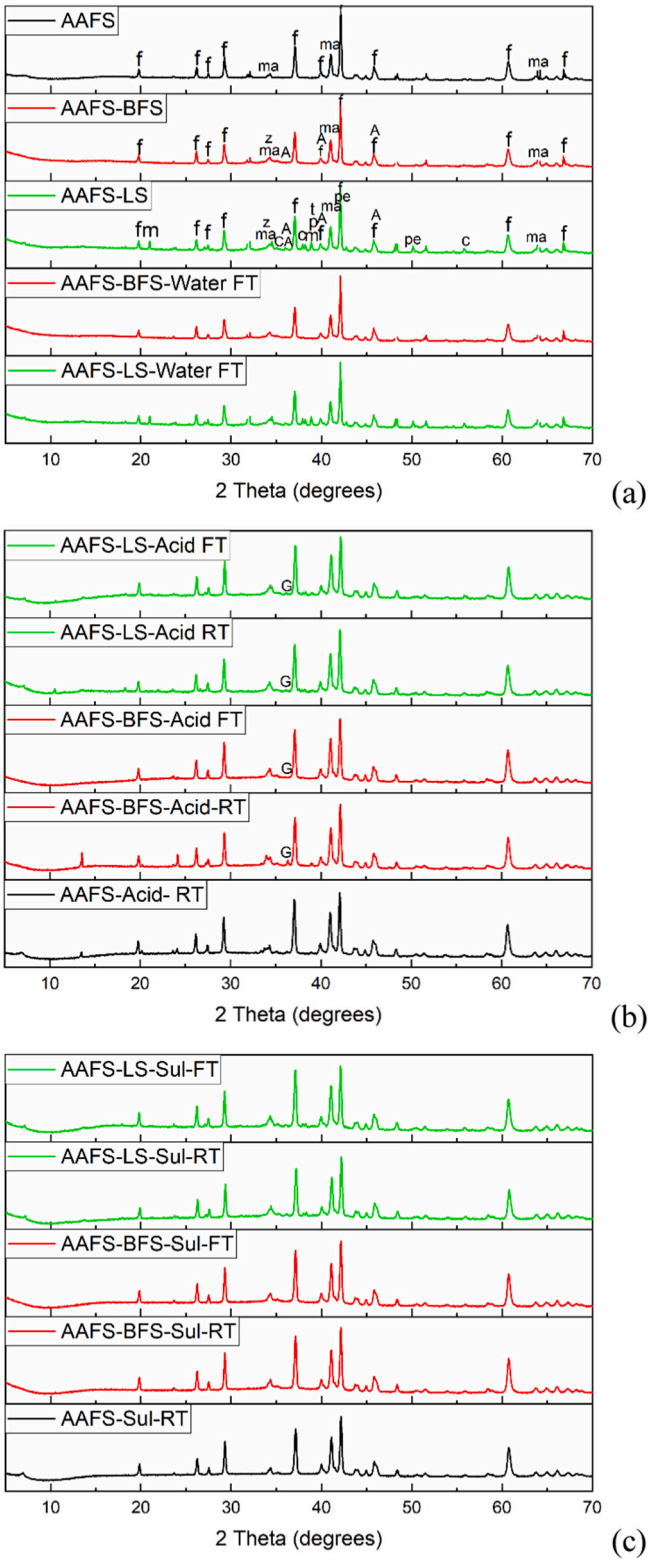

Fig. 8. XRD patterns of AAFS, AAFS-BFS and AAFS-LS: (a) before and after exposure to freeze-thaw cycles in water, (b) after freeze-thaw cycles and immersion at room temperature in acid solution, (c) after freeze-thaw cycles and immersion at room temperature in combined sodium sulfate and chloride solution.

Table 5
Results of QXRD analysis. AAFS (before exposure), AAFS-Sul-RT (after exposure to combined sulfate and chloride at room temperature), AAFS-Acid RT (after exposure to sulfuric acid solution at room temperature).

Sample name	Fayalite	Magnetite	Amorphous
AAFS	32.9	3.3	63.9
AAFS-Sul-RT	36	3.9	58.2
AAFS-acid RT	42	5	53

may cause physical damages via volume expansion and eventually cracks in material structure [40]. Meanwhile, the use of co-binders improved the stability of the blended mortars. The incorporation of co-binder is presumed to have enhanced the degree of binder gel formation, resulting in highly compact and dense binder gel network, which is able to resist the dual effect of freeze-thaw and acid attack. The positive effect of co-binder addition was also visible in mortar samples immersed in sulfuric acid solution at room temperature, with the AAFS-LS and AAFS-BFS having higher compressive strength after exposure compared to AAFS. Comparatively, higher strength was retained in samples exposed to acid solution at room temperature compared to their counterparts subjected to freeze-thaw cycles in acid solution, consistent with the mass loss results in Fig. 6. After 60 days immersion in acid solution at room temperature, the compressive strength of AAFS-LS, AAFS-BFS and AAFS was 23, 22 and 9 MPa, respectively (Fig. 7b).

On the other hand, the strength loss by samples after exposure to combined sulfate and chloride attack is mostly due to the movement of ions inherent in them. When the samples is immersed in sulfate and chloride solution, the infiltration of sulfate and chloride ions can induce chemical volume changes throughout the material as a result of the reaction between these ions and cementitious materials [40]. In blended mortars, the incorporation of co-binders played a critical role in terms of controlling the crack development and eventually minimizing degradation of the mechanical properties under freeze-thaw and chemical attacks. Thus, blended mortars exhibited higher resistance to combined sulfate and chloride attack compared to AAFS. After exposure to 180 freeze-thaw cycles in combined sulfate and chloride solution, the compressive strength of AAFS-LS, and AAFS-BFS decreased to 20 and 17 MPa respectively while that of AAFS could not be measured due to complete damage (Fig. 7c). It is possible that the deteriorative chemical reaction between the solution and mortar components under freeze-thaw conditions resulted in the rapid production of expansive agents, thus causing severe deterioration in AAFS. Similar observation has also been reported in unreinforced ettringite-based binder after 180 freeze-thaw cycles in combined sodium sulfate and chloride solution [40]. However, strength reduction rate was lower when the samples were immersed in combined sulfate and chloride solution and placed at room temperature. After 60 days of exposure in combined sulfate and chloride solution at room temperature, the compressive strength of AAFS-LS, AAFS-BFS and AAFS was 41, 28, and 13 MPa, respectively, (Fig. 7d); the strength of blended samples meets the requirements of many design codes such as Euro code 2 [48]. The superior compressive strength observed in all samples immersed in combined sulfate and chloride solution at room temperature compared to their counterpart in freeze-thaw conditions is consistent with their lower deterioration level observed in Fig. 4.

Furthermore, the loss of mechanical strength by samples after exposure to freeze-thaw conditions in water is likely due to the volume expansion of absorbed water in pores. Also, it is well known phenomenon that the infiltration of water molecules inside the pore cavities of AAM weakens its structure resulting in lower mechanical properties. The absorption of this water is likely to increase with time especially in samples that is more porous (see porosity in Section 3.6). After 180 freeze-thaw cycles in water, the compressive strength of AAFS-LS and AAFS-BFS decreased to 30 and 20 MPa, respectively, while that of AAFS could not be determined due to severe deterioration (Fig. 7e). One possible explanation could be that the formation of a close-grained reaction product in blended mortars makes it difficult for water to penetrate and difficult for mortar to become frozen and saturated, thus making AAFS-LS and AAFS-BFS mortar more durable. The residual compressive strength of blended mortars is as good as those reported for alkali-activated soapstone waste or other low-calcium FA-based geopolymers and also satisfied the minimum requirements specified for building materials subjected to severe weathering conditions [39,49]. Overall, these results confirmed the role of co-binders in terms of improving the durability of low reactive FS-based mortars. The better stability of blended mortars under physical, chemical, and combined physical and chemical attacks suggests that they possess a potential to withstand mild and severe weathering conditions, resulting in the development of a strong and compact matrix.

In addition, the residual compressive strength of all the mortar samples during wet and dry conditions is presented in Table 4. It can be seen that there is a slight reduction in the strength values of all the

Table 6
Results of QXRD analysis. AAFS-BFS (before exposure), AAFS-BFS-water-FT (after exposure to freeze-thaw in water), AAFS-BFS-acid FT (after exposure to freeze-thaw in sulfuric acid solution), AAFS-BFS-acid RT (after exposure to sulfuric acid solution at room temperature), AAFS-BFS-Sul FT (after exposure to freeze-thaw cycles in combined sulfate and chloride solution), AAFS-BFS-Sul RT (after exposure to combined sulfate and chloride solution at room temperature).

Sample name	Fayalite	Magnetite	Calcite	Andradite	Gypsum	Amorphous
AAFS-BFS	30.9	3.6	2.8	2.6		60.1
AAFS-BFS-water FT	31	3.5	2.9	2.6		60
AAFS-BFS-acid FT	42	6	0.5	0.9	7	43.6
AAFS-BFS-acid RT	40	4	0.9	1.2	5	48.9
AAFS-BFS-Sul FT	34	5	2.2	2		56.8
AAFS-BFS-Sul RT	33	4	2.5	2.3		58.2

Table 7
Results of QXRD analysis. AAFS-LS (before exposure), AAFS-LS-water-FT (after exposure to freeze-thaw in water), AAFS-LS-acid FT (after exposure to freeze-thaw in sulfuric acid solution), AAFS-LS-acid RT (after exposure to sulfuric acid solution at room temperature), AAFS-LS-Sul-FT (after exposure to freeze-thaw cycles in combined sulfate and chloride solution), AAFS-LS-Sul-RT (after exposure to combined sulfate and chloride solution at room temperature).

Sample name	Fayalite	Magnetite	Mayenite	Perovskite	C_3A	Q-phase	Gypsum	Periclase	γ - C_2S	Calcite	Andradite	Amorphous
AAFS-LS	26.3	2.9	1.1	1.8	0.1	8.7		6.9	1.8	4	2	44.4
AAFS-LS-water FT	26	3	1.1	1.8	0.1	7.9		6.9	2.8	3.9	2	44.5
AAFS-LS-acid FT	38	5					10	9	9	1.5	0.5	27
AAFS-LS-acid-RT	36	4					9	8	8	2	0.8	32.2
AAFS-LS-Sul-FT	33	4						8.8	7	3.5	1.5	42.2
AAFS-LS-Sul-RT	32.9	3.2						8.5	6	3.7	1.7	44

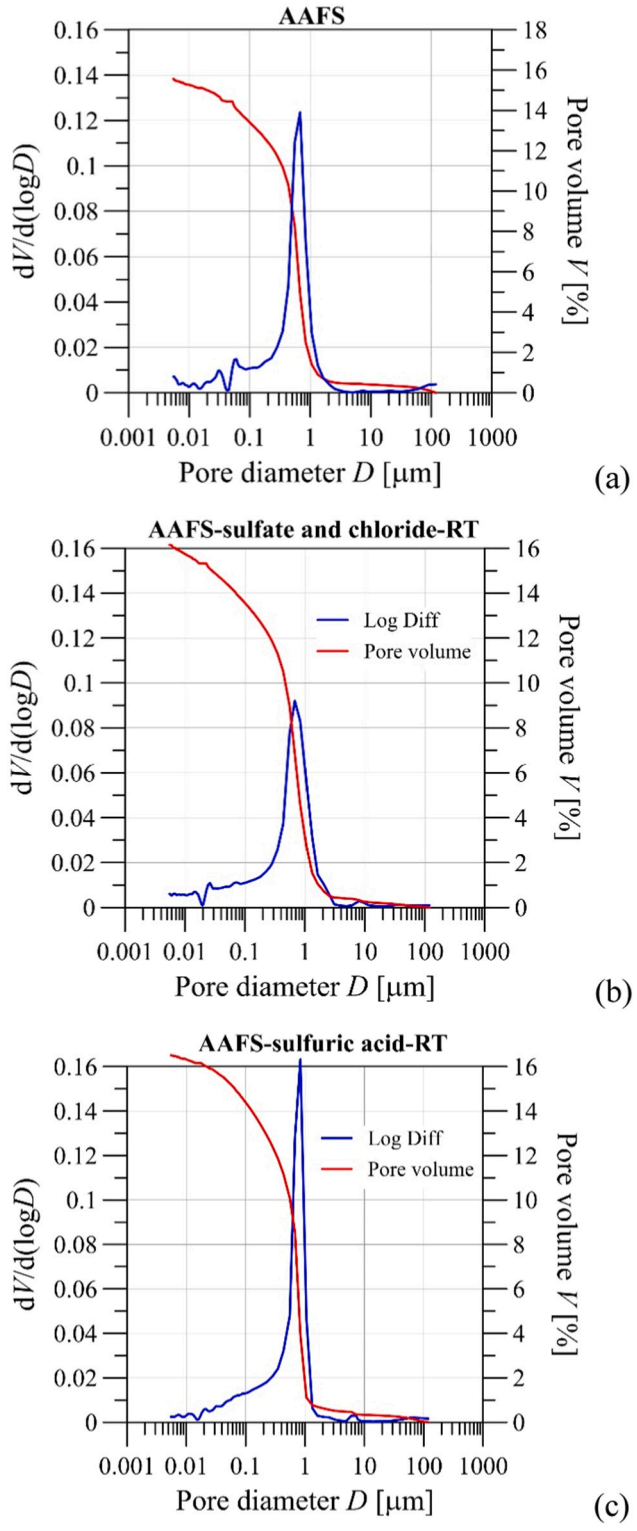

Fig. 9. Porosity of AAFS before and after exposure to aggressive environments: (a) AAFS before exposure, (b) AAFS after exposure to combined sulfate and chloride solution at room temperature for 60 days, (c) AAFS after exposure to sulfuric acid solution at room temperature (RT) for 60 days.

mortar samples after 60 days. Furthermore, no visual deterioration (not shown here) was observed on the surface of all the samples, indicating that all the mortar samples are stable under drying and wetting conditions and can be suitable for dry and wet environments.

3.5. XRD analysis

The XRD patterns of AAFS, AAFS-BFS and AAFS-LS before and after exposure to different environmental conditions are presented in Fig. 8. Before exposure, AAFS showed similar mineralogical composition as the raw FS; Fayalite [(Fe_2SiO_4) pdf. 04-007-9022] and magnetite [(Fe_3O_4) pdf. 04-008-8145] were the main identified crystalline phases. No newly formed crystalline phase was identified in AAFS which indicate the formation of mainly amorphous phase. Meanwhile, the mineralogical composition of AAFS-BFS is slightly different from those observed for AAFS. The crystalline phases identified were fayalite, magnetite, andradite [($Ca_3Fe_2(SiO_4)_3$ pdf. 04-013-6178] and calcite [($CaCO_3$) pdf. 04-006-6528] (Fig. 8 and Table 6). Fayalite and magnetite originated from the initial FS while calcite and andradite appeared after alkali activation. The appearance of calcite is attributed to carbonation of the samples during curing while the formation of andradite is mainly due to the interaction between dissolved Fe and Si in FS and calcium silicate phases in BFS, consistent with those reported in previous study [50]. As for AAFS-LS, most of the initial crystalline phases present in the precursor samples of FS and LS remained after alkali activation. However, there was a significant reduction in some crystalline phases, suggesting partly transformation into an amorphous structure after alkali activation. The phases present after activation included fayalite, magnetite, mayenite [($C_{12}A_7$) pdf. 04-015-5594], periclase [(MgO) pdf. 04-002-2876], perovskite [($CaTiO_3$) pdf. 04-005-5587], tricalcium aluminate [(C_3A) pdf. 04-007-4797], calcium aluminium magnesium silicate [Q phase pdf. 04-009-3800] and calcio-olivine [(γ - C_2S) pdf. 04-006-8894] (Fig. 8 and Table 7). Calcite and andradite appeared as the new crystalline phase in AAFS-LS and their formation is similar to those observed in AAFS-BFS.

Meanwhile, after exposure to 180 freeze-thaw cycles in water, the XRD analysis of AAFS could not be measured due to complete disintegration. However, the XRD analysis of AAFS-LS and AAFS-BFS after exposure to freeze-thaw cycles in water shows no significant difference when compared to its corresponding unexposed samples, indicating that the difference in properties of the samples before and after exposure is largely influenced by physical attack (i.e., volume expansion due to water uptake) (see Fig. 8, Tables 6, and 7). On the other hand, physical and chemical attacks are the main factor causing disintegration in materials immersed in acid and combined sulfate and chloride solution. The XRD results of AAFS samples after immersion in sulfuric acid solution for 60 days at room temperature showed a slight increase in the crystalline intensities of fayalite and magnetite while the amorphous content decreased in comparison to unexposed samples (Table 5). The increase in crystalline contents may likely be attributed to the decomposition of AAM gel after acid exposure. Similarly, AAFS-LS undergone significant changes after exposure to acid solution. The XRD results of AAFS-LS samples immersed in acid solution for 60 days at room temperature showed a slight decrease in amorphous content (Table 7). As AAFS-LS was exposed to freeze-thaw cycles in sulfuric acid solution, the decrease in the amorphous content intensifies. One possible explanation for significant reduction in amorphous content of AAFS-LS exposed to freeze-thaw cycles in acid solution compared to those exposed to acid solution and placed at room temperature may likely be due to freeze-thaw effect which enhances chemical diffusion process, resulting in higher decomposition of gel. Compared to the unexposed samples of AAFS-LS, mayenite, tricalcium aluminate, perovskite, calcium aluminium magnesium silicate peaks disappeared, while the crystalline intensities of periclase, calcio olivine, fayalite and magnetite increased. Besides, calcite, andradite and amorphous content decreased, and a new crystalline phase of gypsum [($CaSO_4{\cdot}2H_2O$) pdf. 00-033-0311] was formed in the specimen. Also, the XRD results of AAFS-BFS showed a decrease in the amorphous content after immersion in acid solution at room temperature for 60 days. Meanwhile, exposure of similar samples to freeze-thaw cycles in acid solution further decreased the amorphous content. After exposure, fayalite and magnetite content increased while

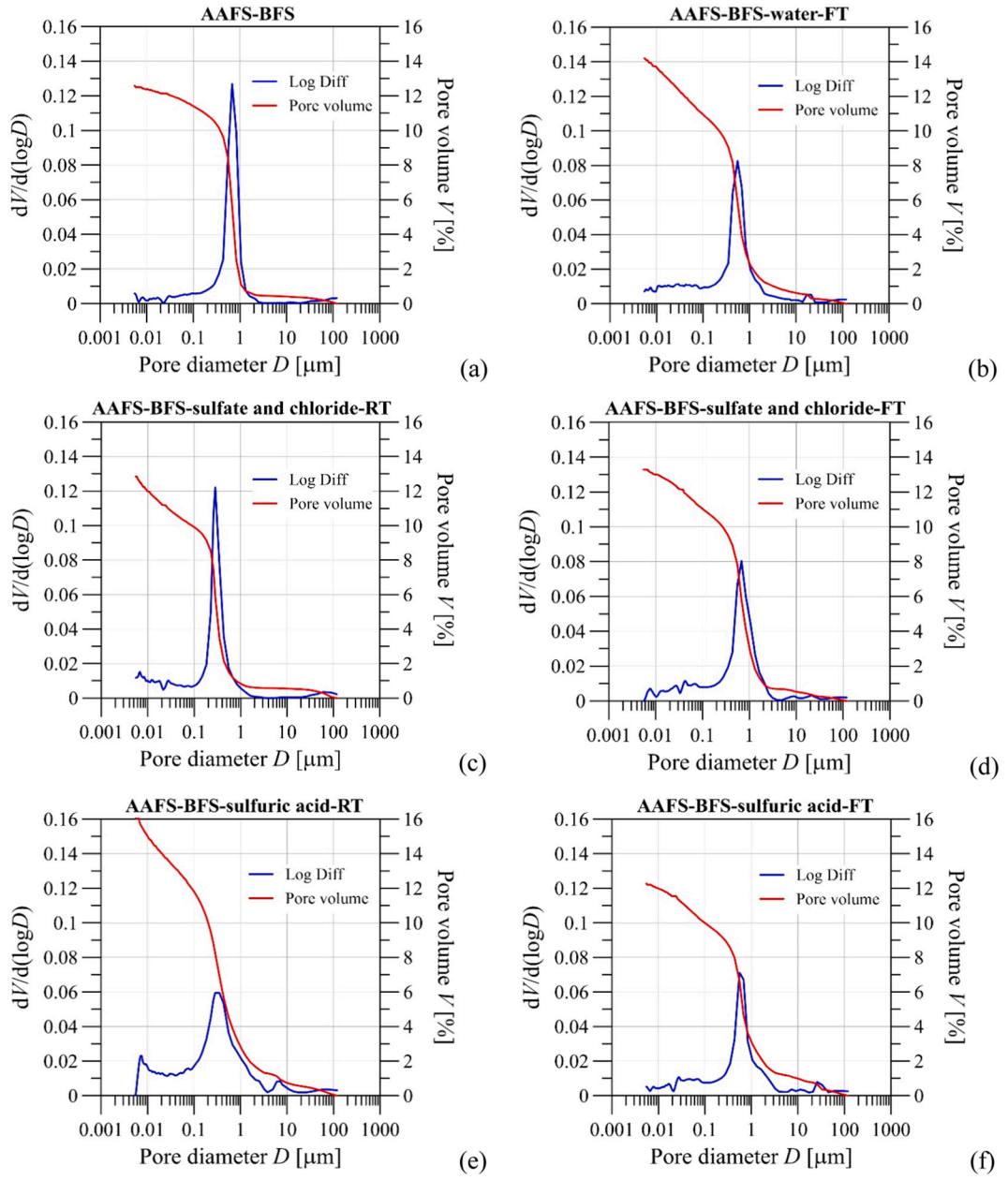

Fig. 10. Porosity of AAFS-BFS before and after exposure to aggressive environments: (a) AAFS-BFS before exposure, (b) AAFS-BFS after exposure to 180 freeze-thaw (FT) cycles in water, (c) AAFS-BFS after exposure to combined sulfate and chloride solution at room temperature (RT) for 60 days, (d) AAFS-BFS after exposure to 180 freeze-thaw cycles in combined sulfate and chloride solution, (e) AAFS-BFS after exposure to sulfuric acid solution at room temperature for 60 days, (f) AAFS-BFS after exposure to 180 freeze-thaw cycles in sulfuric acid solution.

calcite, andradite and amorphous content decreased. Besides, a new crystalline phase of gypsum was formed in the specimens. The formation of gypsum in AAFS-BFS and AAFS-LS is attributed to incorporation of LS and BFS which contains higher amounts of calcium, facilitating their reaction with sulfuric acid. However, the lower quantity of gypsum formed does not have a significant influence on the mechanical properties.

Furthermore, it was observed that the exposure of AAFS, AAFS-BFS and AAFS-LS to combined sulfate and chloride solution caused slight changes in their XRD results when compared to their corresponding unexposed samples. The XRD results of AAFS exposed to freeze-thaw cycles in combined sulfate and chloride solution could not be measured due to disintegration, but that of AAFS exposed to combined sulfate and chloride solution at room temperature showed an increase in the crystalline content of fayalite and magnetite while the amorphous content slightly decreased (Table 5). Moreover, in AAFS-LS, mayenite, tricalcium aluminate, perovskite, and calcium aluminium magnesium silicate was no longer present in their XRD after exposure to combined sulfate and chloride solution, suggesting that these crystalline phases are vulnerable to combined sulfate and chloride attack. Besides, fayalite, magnetite and periclase content increased while calcite, andradite, and the amorphous content decreased. For similar samples exposed to freeze-thaw cycles in combined sulfate and chloride solution, the joint effect of freeze-thaw and chemical uptake is presumed to have influenced the mineralogical composition leading to further reduction in the amorphous content (Table 7). In addition, the calcite, andradite, and amorphous content of AAFS-BFS decreased after exposure to combined sulfate and chloride solution in freeze-thaw cycles and room temperature, while the content of fayalite and magnetite increased when compared to unexposed samples (Table 6).

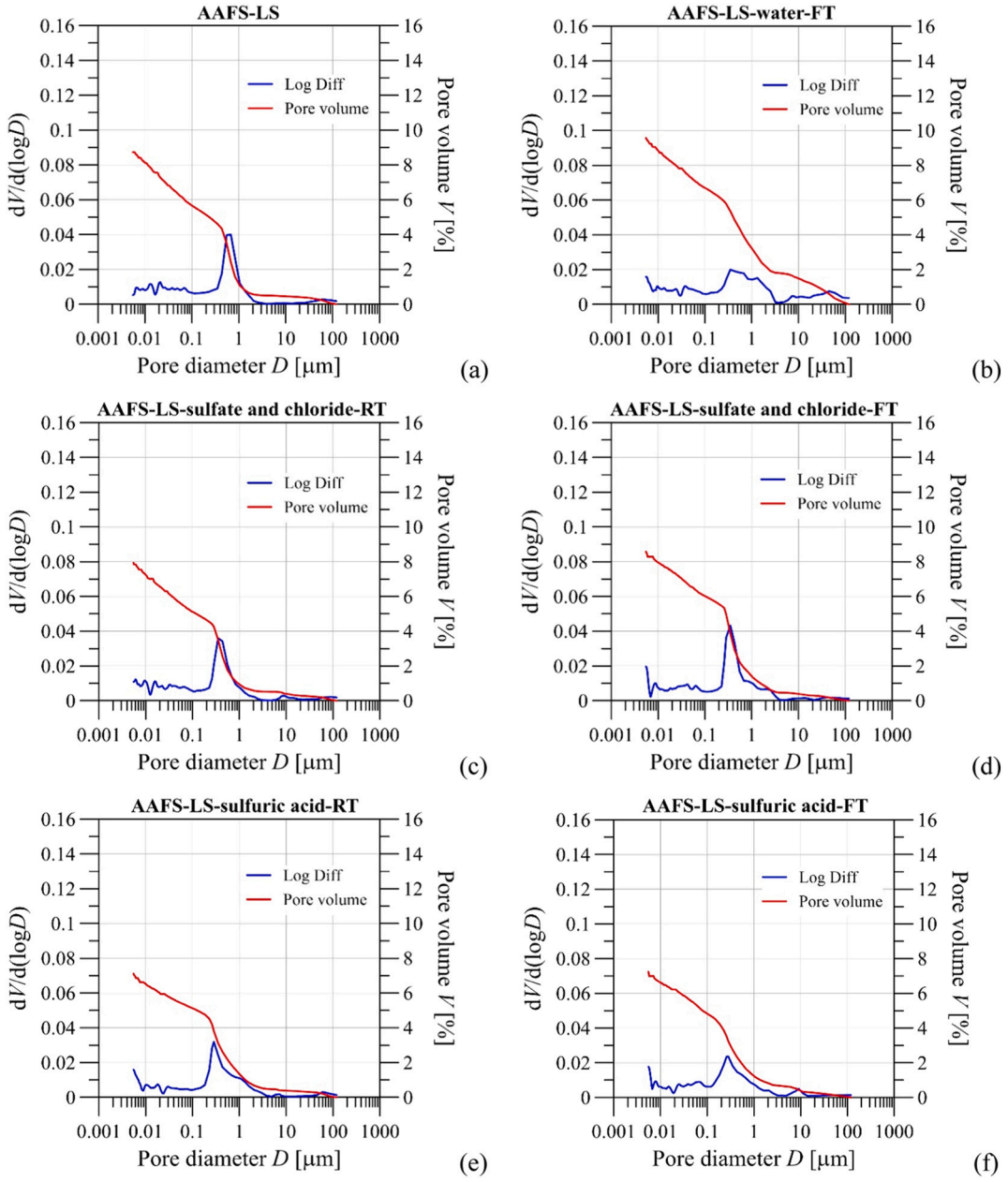

Fig. 11. Porosity of AAFS-LS before and after exposure to aggressive environments: (a) AAFS-LS before exposure, (b) AAFS-LS after exposure to 180 freeze-thaw (FT) cycles in water, (c) AAFS-LS after exposure to combined sulfate and chloride solution at room temperature (RT) for 60 days, (d) AAFS-LS after exposure to 180 freeze-thaw cycles in combined sulfate and chloride solution, (e) AAFS-LS after exposure to sulfuric acid solution at room temperature for 60 days, (f) AAFS-LS after exposure to 180 freeze-thaw cycles in sulfuric acid solution.

Meanwhile, the role of chloride in the combined sulfate and chloride solution needs further investigation. As reported in literature, the presence of chloride in the solution could delay the sulfate diffusion due to high diffusion rate of chloride to form Friedel's salt ($C_3A{\cdot}CaCl_2{\cdot}10H_2O$), which mainly results from the interaction between chloride and Al-rich phases [51]. However, lack of detection of this salt by XRD in this study may likely be due to their amount being below the detection limit. In general, the XRD results of all the samples after exposure to combined sulfate and chloride solution in freeze-thaw cycles and room temperature did not produce any new crystalline phases.

3.6. Porosity

The porosity of the mortar samples before and after exposure to different environmental conditions is presented in Figs. 9, 10 and 11. Before exposure, AAFS (Fig. 9a) exhibited the highest porosity among all the mixes, followed by AAFS-BFS (Fig. 10a), with the lowest porosity occurring in AAFS-LS (Fig. 11a). The reason for lower porosity in AAFS-LS and AAFS-BFS is due to the incorporation of LS and BFS which refines the pore structure and is presumed to be one of the primary reasons for their denser microstructure (see Section 3.7) and higher initial compressive strength (see Fig. 7). Meanwhile, it was observed that the addition of LS as co-binder was more effective in reducing the porosity than BFS, suggesting that different co-binders have different impact on the pore structure refinement; AAFS-LS having the least porosity exhibited highest compressive strength. This observation is consistent with a previous study where lower porosity and higher compressive strength was reported when alkali-activated copper slag was blended with metakaolin and FA in comparison to the neat copper slag [52]. After exposure to sulfuric acid solution at room temperature, the

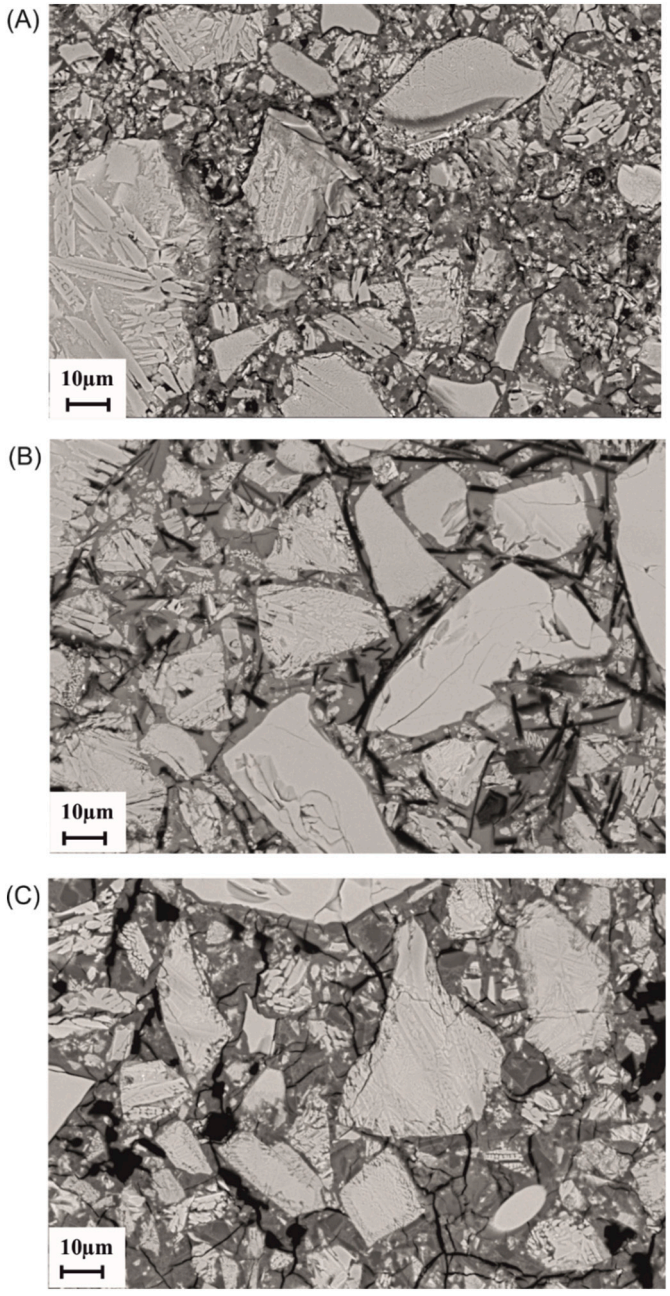

Fig. 12. Backscattered electron imaging of AAFS before and after exposure to aggressive environments: (a) AAFS before exposure, (b) AAFS after exposure to sulfuric acid solution at room temperature for 60 days, (c) AAFS after exposure to combined sulfate and chloride solution at room temperature for 60 days.

porosity of AAFS (Fig. 9c) and AAFS-BFS (Fig. 10e) increased while that of AAFS-LS (Fig. 11e) decreased when compared to the unexposed samples. Meanwhile, there is almost no difference in the porosity values of AAFS-LS immersed in freeze-thaw cycles in acid solution (Fig. 11f) when compared to similar samples immersed in acid solution at room temperature (Fig. 11e). Compared to their corresponding unexposed samples, the porosity of AAFS (Fig. 9b) increased while that of AAFS-LS (Fig. 11c) and AAFS-BFS (Fig. 10c) remain almost unchanged or slightly decreased after immersion in combined sulfate and chloride solution at room temperature. Similarly, after exposure to combined sulfate and chloride solution in freeze-thaw, the porosity of AAFS-BFS (Fig. 10d) and AAFS-LS (Fig. 11d) remain almost unchanged when compared to their counterparts immersed in combined sulfate and chloride solution and placed at room temperature. Furthermore, the porosity of AAFS-LS (Fig. 11b) and AAFS-BFS (Fig. 10b) slightly increased after exposure to freeze-thaw cycles in water when compared with the unexposed samples. Overall, the changes in porosity values are more evident in AAFS after exposure to different environmental conditions compared to AAFS-LS and AAFS-BFS, and this may likely be related to the binding gel formed in each system. Sodium iron silicate (N-F-S) gel mostly formed in AAFS mixes is less dense and more porous than a mix of C-A-S-H, C-(N)-A-S-H and N-F-S gels formed in AAFS-LS and AAFS-BFS (see Section 3.7). The binder gels formed in AAFS-LS and AAFS-BFS contributed to the pore structure refinement and strength development, consistent with those reported in the literature where an appropriate mix of C-A-S-H and N-A-S-H gels favoured pore structure development and mechanical performance of geopolymers [53].

3.7. SEM-EDS

The SEM micrographs of the representative sections of alkali-activated mortar samples before and after exposure to different environmental conditions are presented Figs. 12, 13 and 14. Before exposure, AAFS is characterized by poor binder gel formation with large number of unreacted particles embedded in the matrix as aggregates (Fig. 12a), consistent with those reported in previous study [22]. Comparatively, AAFS-BFS and AAFS-LS displayed denser and more homogenous microstructure, attributed to higher extent of reaction of the precursors, and accelerated binder gel formation (Fig. 13a and 14a). This observation agrees with compressive strength development, which is higher for blended mortars (see Section 3.4). After exposure to sulfuric acid and combined sulfate and chloride solution at room temperature for 60 days, AAFS-LS and AAFS-BFS exhibited more compact microstructure and good bonding between the aggregate and the binder gel compared to AAFS (Fig. 12b, c, 13c, e, 14c, e). This difference in the microstructure confirms the role of co-binders in slowing down the chemical attacks due to exposure to acid solution and combined sulfate and chloride solution. On the other hand, the micrographs of AAFS-LS and AAFS-BFS samples exposed to freeze-thaw cycles in water showed visible microcracks compared to their corresponding unexposed samples, attributed to the freeze-thaw effect (physical attack) which induces microcracks in the structure (Fig. 13a, b, 14a, b). Moreover, AAFS-LS and AAFS-BFS after exposure to 180 freeze-thaw cycles in combined sulfate and chloride solution is presumed to have reacted with the environment, resulting in the weakening of the binder gel and crack formation. Additionally, the micrographs of AAFS-LS and AAFS-BFS exposed to 180 freeze-thaw cycles in acid solution are characterized with several pores and microcracks along the edges of unreacted particle in the matrix; attributed to the combined physical and chemical attacks which eventually extend the microcracks into the material. The joint effect of freeze-thaw and chemical solution is presumed to have caused rapid continuous deterioration of the samples and diffusion of soluble compounds, causing enlargement of pore space, resulting in deeper solution penetration and thus influenced the specimen integrity. The microstructural changes of the mortar specimens before and after exposure to different environmental conditions indicated strength degradation observed in Fig. 7.

The EDS results obtained from 150 randomly selected points in the bulk binder gel of AAFS, AAFS-LS and AAFS-BFS before and after exposure to different environmental conditions are presented in Table 8. Ca, Al, Fe, Si and Na contents of the specimens were reported and used for determining the chemical ratios (Table 8) and plot the ternary diagrams (see Fig. A.1 in supplementary information). Table 8 and the ternary plots (Fig. A.1) clearly show a variation in the binder gel composition of the blended samples when compared to the reference sample. The average atomic ratio values of the binder gel demonstrated that AAFS has higher concentration of Fe/Si with lower Ca/Si and Al/Si when compared to AAFS-LS and AAFS-BFS, consistent with the raw material compositions (Table 1). The binder gel of AAFS shows higher content of Fe, indicating that Fe-containing glass in FS can undergo dissolution in alkaline media. The binder gel formed in AAFS is mainly

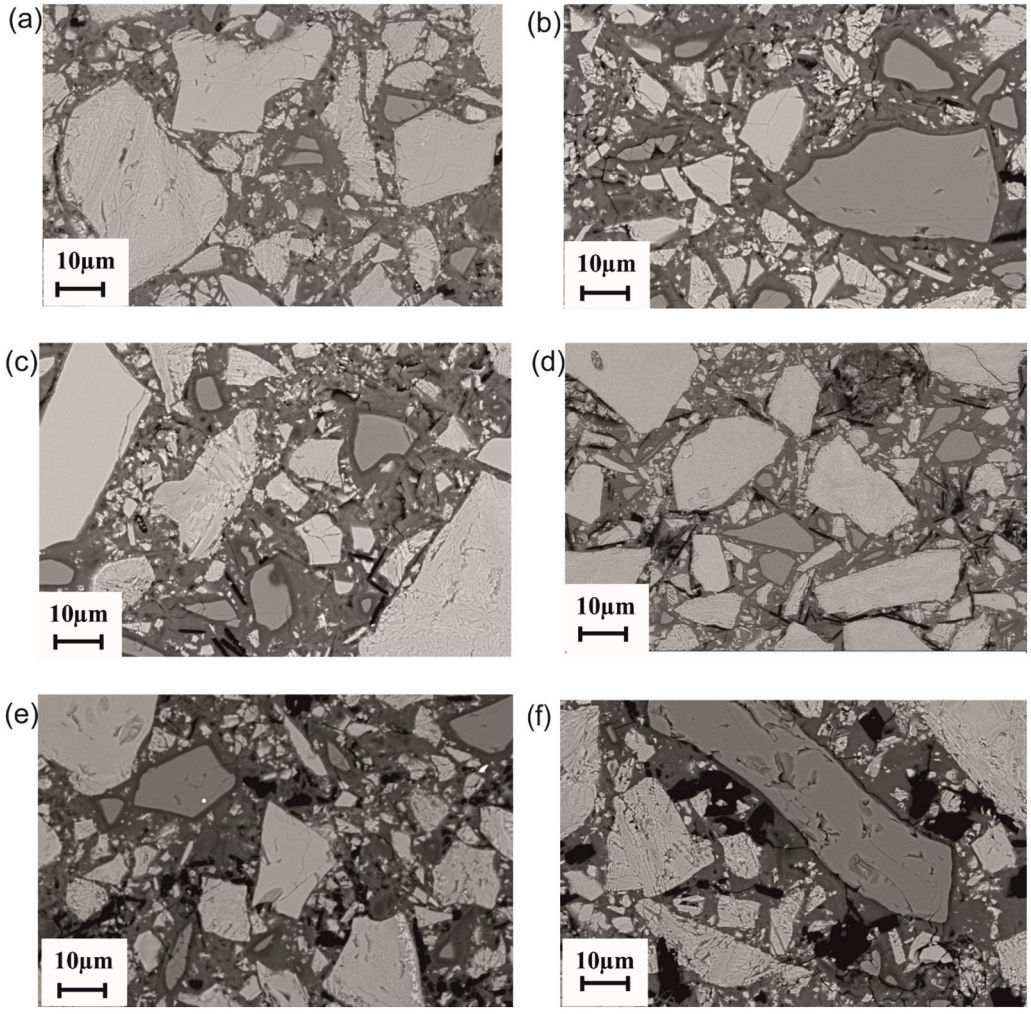

Fig. 13. Backscattered electron imaging of AAFS-BFS before and after exposure to aggressive environments: (a) AAFS-BFS before exposure, (b) AAFS-BFS after exposure to 180 freeze-thaw cycles in water, (c) AAFS-BFS after exposure to combined sulfate and chloride solution at room temperature for 60 days, (d) AAFS-BFS after exposure to 180 freeze-thaw cycles in combined sulfate and chloride solution, (e) AAFS-BFS after exposure to sulfuric acid solution at room temperature for 60 days, (f) AAFS-BFS after exposure to 180 freeze-thaw cycles in sulfuric acid solution.

N-F-S gel (Table 8 and Fig. A.1) and this agrees with the Fe behavior during alkali activation of iron rich slags with low Ca and Al contents [24,27,54]. Higher Ca-content observed with the addition of LS or BFS, indicated the incorporation of this element in the gel structure and this appears to be important for strength development and stronger bonding in AAFS-LS and AAFS-BFS (see Sections 3.4 and 3.7). On the other hand, Al/Si ratios was higher in AAFS-LS, indicating Al originating mainly from LS dissolved in alkaline environment and preferably incorporates into the structure which contributes to the formation of AAM gel and hence higher strength development compared to AAFS-BFS. In both AAFS-LS and AAFS-BFS, a possible formation of a mix of C-A-S-H, C-(N)-A-S-H and N-F-S is presumed to have occurred, consistent with those identified in BFS/FA blends and slag/volcanic ash blends where a mix of C-A-S-H and N-A-S-H gel was observed in the binder gel [55,56]. For AAFS-LS and AAFS-BFS samples exposed to acid solution at room temperature and freeze-thaw conditions, the Ca/Si ratio decreased compared to the unexposed samples, likely due to decalcification, causing calcium to leach from the mortar matrix into acid solutions [11], resulting in decrease in compressive strength observed in Section 3.4. Also, the decrease in Al/Si ratio of AAFS-BFS and AAFS-LS after exposure to acid solution, can be ascribed to the dealumination of the binder gel. Exposure of the samples to strong acid such as sulfuric acid can cause dealumination of the aluminosilicate structure and breakage of Si-O-Al bonds [11]. Furthermore, the exposure of AAFS-LS and AAFS-BFS to combined sulfate and chloride solution at room temperature and at freeze-thaw conditions also caused a slight decrease in the Ca/Si ratio. The Al/Si ratio of AAFS-BFS remain unchanged before and after exposure to combined sulfate and chloride solution while that of AAFS-LS slightly decreased after exposure. Meanwhile, significant amount of Al/Si was retained in AAFS-LS after exposure, indicating that cross-linked aluminosilicate gels formed were more stable in acid solution and combined sulfate and chloride solution.

4. Conclusions

This experimental study investigated the durability properties of Fe-rich fayalite slag-based AAMs. The effect of LS or BFS addition on the shrinkage and exposure to physical, chemical, and combined physical and chemical attacks representing different environmental conditions in cold and tropical regions was assessed. The results showed that the incorporation of LS or BFS slightly increased the drying shrinkage and enhanced the durability of the blended mortars when subjected to different environmental conditions. Blended mortars displayed better stability regardless of the exposure period and environments. The pore refining effect of incorporated LS or BFS lowered the diffusion of water, acid, sulfate, and chloride ions into the matrix which subsequently lowered the volume expansion caused by physical (freeze-thaw cycles), chemical (acid and sodium sulfate + sodium chloride) and combined physical and chemical (freeze-thaw + acid, freeze-thaw + sodium sulfate and chloride) attacks. Meanwhile, exposure of blended mortars to freeze-thaw cycles in water, acid and combine sulfate and chloride presented different properties in comparison to their counterparts immersed in similar solutions and placed at room temperature. The blended mortars subjected to freeze-thaw cycles in water, acid and

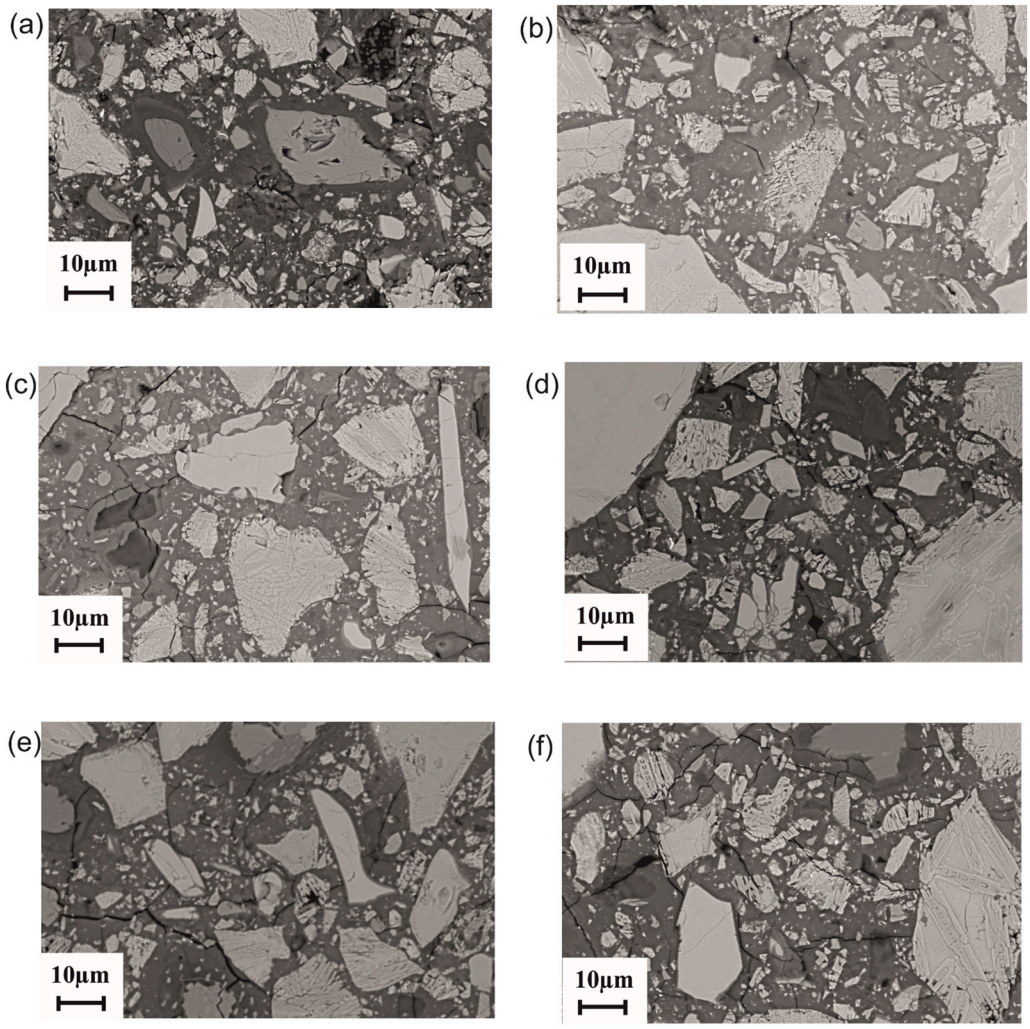

Fig. 14. Backscattered electron imaging of AAFS-LS before and after exposure to aggressive environments: (a) AAFS-LS before exposure, (b) AAFS-LS after exposure to 180 freeze-thaw cycles in water, (c) AAFS-LS after exposure to combined sulfate and chloride solution at room temperature for 60 days, (d) AAFS-LS after exposure to 180 freeze-thaw cycles in combined sulfate and chloride solution, (e) AAFS-LS after exposure to sulfuric acid solution at room temperature for 60 days, (f) AAFS-LS after exposure to 180 freeze-thaw cycles in sulfuric acid solution.

Table 8
Representative EDS results describing the average elemental composition of the binder gel of mortar samples before and after exposure to different environmental conditions.

	Ca/Si	Al/Si	Fe/Si	Na/Si
AAFS	0.14	0.12	0.65	0.19
AAFS-BFS	0.65	0.18	0.23	0.13
AAFS-LS	0.66	0.43	0.64	0.76
AAFS-acid-RT	0.10	0.12	0.61	0.18
AAFS-Sul-RT	0.06	0.11	0.53	0.35
AAFS-BFS-acid RT	0.37	0.16	0.21	0.23
AAFS-BFS-acid FT	0.41	0.14	0.26	0.25
AAFS-BFS-Sul RT	0.52	0.18	0.91	0.25
AAFS-BFS-Sul FT	0.40	0.17	0.22	0.35
AAFS-LS-acid RT	0.54	0.32	0.37	0.26
AAFS-LS-acid FT	0.43	0.37	0.52	0.37
AAFS-LS-Sul RT	0.58	0.31	0.67	0.31
AAFS-LS-Sul FT	0.45	0.34	0.62	0.37
AAFS-BFS-water FT	0.37	0.14	0.30	0.24
AAFS-LS-water FT	0.53	0.28	0.71	0.31

combined sulfate and chloride solution exhibited higher mass loss and strength reduction rate compared to their counterparts immersed in similar solutions and placed at room temperature. On the other hand, sole FS-based mortars exhibited poor durability after exposure to aggressive conditions and were completely deteriorated, particularly those exposed to freeze-thaw cycles in water, acid and combined sulfate and chloride solution. Sole FS-based AAMs was stable during dry and wet conditions and when exposed to acid solution and combined sulfate and chloride solution at room temperature but was destroyed after 90 freeze-thaw cycles in water, acid solution and combined sulfate and chloride solution, attributed to the volume expansion caused by frost and chemical attacks. Microstructural characterization revealed that the incorporation of LS or BFS influences the mortar morphology, element distribution and enhanced the resistance to aggressive environmental conditions which in turn affects the dimensional stability of the mortars and their properties. The decomposition of the gel was considerably significant particularly in samples exposed to combined physical and chemical attacks, but improved stability and higher strength was retained in samples containing LS or BFS. This further proves that the incorporation of BFS or LS can help to reduce material deterioration and hence increase the durability properties of FS-based mortars. Overall, this study contributes to understanding the durability of alkali-activated FS and alkali-activated FS composite subjected to different environmental conditions.

Supplementary data to this article can be found online at https://doi.org/10.1016/j.cemconres.2022.106984.

CRediT authorship contribution statement

Adeolu Adediran: Conceptualization, Methodology, Validation, Formal analysis, Investigation, Visualization, Writing – original draft, Writing – review & editing. **Juho Yliniemi:** Conceptualization,

Methodology, Validation, Writing – review & editing, Funding acquisition, Project administration. **Valter Carvelli:** Conceptualization, Methodology, Validation, Writing – review & editing. **Elijah Adesanya:** Conceptualization, Methodology, Validation, Writing – review & editing. **Mirja Illikainen:** Conceptualization, Writing – review & editing, Funding acquisition, Project administration.

Declaration of competing interest

The authors declare that they have no known competing financial interests or personal relationships that could have appeared to influence the work reported in this paper.

Data availability

Data will be made available on request.

Acknowledgements

This work was done as a part of the TOCANEM project funded by Business Finland and various companies. Adeolu Adediran has received funding from Walter Ahlström and Auramo-säätiö for his doctoral research. J. Yliniemi acknowledge financial support from the Academy of Finland (grant # 322786). The authors gratefully acknowledge the Centre for Material Analysis, University of Oulu, Finland, for assistance with data analysis. The authors acknowledge Prof Cristina Tedeschi (Politecnico di Milano) for the MIP measurements and discussion.

References

[1] J.L. Provis, A. Palomo, C. Shi, Advances in understanding alkali-activated materials, Cem. Concr. Res. 78 (Part A) (2015) 110–125, https://doi.org/10.1016/j.cemconres.2015.04.013.
[2] J.L. Provis, Alkali-activated materials, Cem. Concr. Res. 114 (2018) 40–48, https://doi.org/10.1016/j.cemconres.2017.02.009.
[3] D.W. Law, A.A. Adam, T.K. Molyneaux, I. Patnaikuni, Durability assessment of alkali activated slag (AAS) concrete, Mater. Struct. 45 (2012) 1425–1437, https://doi.org/10.1617/s11527-012-9842-1.
[4] K. Arbi, M. Nedeljković, Y. Zuo, G. Ye, A review on the durability of alkali-activated Fly Ash/Slag systems: advances, issues, and perspectives, Ind. Eng. Chem. Res. 55 (2016) 5439–5453, https://doi.org/10.1021/acs.iecr.6b00559.
[5] S.E. Chidiac, D.K. Panesar, Evolution of mechanical properties of concrete containing ground granulated blast furnace slag and effects on the scaling resistance test at 28days, Cem. Concr. Compos. 30 (2008) 63–71, https://doi.org/10.1016/j.cemconcomp.2007.09.003.
[6] O. Karahan, A. Yakupoğlu, Resistance of alkali-activated slag mortar to abrasion and fire, Adv. Cem. Res. 23 (2011) 289–297, https://doi.org/10.1680/adcr.2011.23.6.289.
[7] S. Mundra, S.A. Bernal, M. Criado, P. Hlaváček, G. Ebell, S. Reinemann, G.J. G. Gluth, J. Provis, Steel corrosion in reinforced alkali-activated materials, RILEM Tech. Lett. 2 (2017) 33–39, https://doi.org/10.21809/rilemtechlett.2017.39.
[8] H. Kukko, R. Mannonen, Chemical and mechanical properties of alkali-activated blast furnace slag (F-CONCRETE), Nord. Concr. Res. 1 (1982). https://trid.trb.org/view/196484. (Accessed 30 June 2021).
[9] P.N. Lemougna, A. Adediran, J. Yliniemi, A. Ismailov, E. Levanen, P. Tanskanen, P. Kinnunen, J. Roning, M. Illikainen, Thermal stability of one-part metakaolin geopolymer composites containing high volume of spodumene tailings and glass wool, Cem. Concr. Compos. 114 (2020), 103792, https://doi.org/10.1016/j.cemconcomp.2020.103792.
[10] E. Adesanya, A. Aladejare, A. Adediran, A. Lawal, M. Illikainen, Predicting shrinkage of alkali-activated blast furnace-fly ash mortars using artificial neural network (ANN), Cem. Concr. Compos. 124 (2021), 104265, https://doi.org/10.1016/j.cemconcomp.2021.104265.
[11] T. Bakharev, Resistance of geopolymer materials to acid attack, Cem. Concr. Res. 35 (2005) 658–670, https://doi.org/10.1016/j.cemconres.2004.06.005.
[12] M. Vafaei, A. Allahverdi, P. Dong, N. Bassim, Acid attack on geopolymer cement mortar based on waste-glass powder and calcium aluminate cement at mild concentration, Constr. Build. Mater. 193 (2018) 363–372, https://doi.org/10.1016/j.conbuildmat.2018.10.203.
[13] A. Mardani-Aghabaglou, Ö. Andiç-Çakir, K. Ramyar, Freeze–thaw resistance and transport properties of high-volume fly ash roller compacted concrete designed by maximum density method, Cem. Concr. Compos. 37 (2013) 259–266, https://doi.org/10.1016/j.cemconcomp.2013.01.009.
[14] S. Yin, L. Jing, M. Yin, B. Wang, Mechanical properties of textile reinforced concrete under chloride wet-dry and freeze-thaw cycle environments, Cem. Concr. Compos. 96 (2019) 118–127, https://doi.org/10.1016/j.cemconcomp.2018.11.020.
[15] P.N. Lemougna, A. Adediran, J. Yliniemi, T. Luukkonen, M. Illikainen, Effect of organic resin in glass wool waste and curing temperature on the synthesis and properties of alkali-activated pastes, Mater. Des. 212 (2021), 110287, https://doi.org/10.1016/j.matdes.2021.110287.
[16] C. Fu, H. Ye, K. Zhu, D. Fang, J. Zhou, Alkali cation effects on chloride binding of alkali-activated fly ash and metakaolin geopolymers, Cem. Concr. Compos. 114 (2020), 103721, https://doi.org/10.1016/j.cemconcomp.2020.103721.
[17] T.H. Vu, N. Gowripalan, P. De Silva, A. Paradowska, U. Garbe, P. Kidd, V. Sirivivatnanon, Assessing carbonation in one-part fly ash/slag geopolymer mortar: change in pore characteristics using the state-of-the-art technique neutron tomography, Cem. Concr. Compos. 114 (2020), 103759, https://doi.org/10.1016/j.cemconcomp.2020.103759.
[18] M. Wasim, T.D. Ngo, D. Law, A state-of-the-art review on the durability of geopolymer concrete for sustainable structures and infrastructure, Constr. Build. Mater. 291 (2021), 123381, https://doi.org/10.1016/j.conbuildmat.2021.123381.
[19] D. Zaharaki, K. Komnitsas, V. Perdikatsis, Use of analytical techniques for identification of inorganic polymer gel composition, J. Mater. Sci. 45 (2010) 2715–2724, https://doi.org/10.1007/s10853-010-4257-2.
[20] K. Komnitsas, D. Zaharaki, V. Perdikatsis, Effect of synthesis parameters on the compressive strength of low-calcium ferronickel slag inorganic polymers, J. Hazard. Mater. 161 (2009) 760–768, https://doi.org/10.1016/j.jhazmat.2008.04.055.
[21] K. Komnitsas, D. Zaharaki, V. Perdikatsis, Geopolymerisation of low calcium ferronickel slags, J. Mater. Sci. 42 (2007) 3073–3082, https://doi.org/10.1007/s10853-006-0529-2.
[22] A. Adediran, J. Yliniemi, M. Illikainen, Development of sustainable alkali-activated mortars using fe-rich fayalitic slag as the sole solid precursor, Front. Built Environ. 7 (2021), https://doi.org/10.3389/fbuil.2021.653466.
[23] V. Saari, P. Latostenmaa, J. Yliniemi, K. Ohenoja, Boliden Harjavalta copper and nickel smelter - review of smelter operations, slags and slag valorisation studies, Retrieved from, in: 6th International Slag Valorisation Symposium, 1-5 April 2019, Mechelen, Belgium 2019, 2019, p. 4, www.slag-valorisation-symposium.eu.
[24] A. Adediran, J. Yliniemi, M. Illikainen, Mineralogy and glass content of Fe-rich fayalite slag size fractions and their effect on alkali activation and leaching of heavy metals, Int. J. Ceram. Eng. Sci. 3 (2021) 287–300, https://doi.org/10.1002/ces2.10107.
[25] C. Shi, C. Meyer, A. Behnood, Utilization of copper slag in cement and concrete, Resour. Conserv. Recycl. 52 (2008) 1115–1120, https://doi.org/10.1016/j.resconrec.2008.06.008.
[26] K.L. Scrivener, V.M. John, E.M. Gartner, Eco-efficient cements: potential economically viable solutions for a low-CO2 cement-based materials industry, Cem. Concr. Res. (2018), https://doi.org/10.1016/j.cemconres.2018.03.015.
[27] S. Onisei, A.P. Douvalis, A. Malfliet, A. Peys, Y. Pontikes, Inorganic polymers made of fayalite slag: on the microstructure and behavior of fe, J. Am. Ceram. Soc. 101 (2018) 2245–2257, https://doi.org/10.1111/jace.15420.
[28] S. Onisei, K. Lesage, B. Blanpain, Y. Pontikes, Early age microstructural transformations of an inorganic polymer made of fayalite slag, J. Am. Ceram. Soc. 98 (7) (2015) 2269–2277. http://onlinelibrary.wiley.com/doi/10.1111/jace.13548/full. (Accessed 16 June 2015).
[29] P. Duxson, A. Fernández-Jiménez, J.L. Provis, G.C. Lukey, A. Palomo, J.S.J. van Deventer, Geopolymer technology: the current state of the art, J. Mater. Sci. 42 (2007) 2917–2933, https://doi.org/10.1007/s10853-006-0637-z.
[30] G. Beersaerts, A. Vananroye, D. Sakellariou, C. Clasen, Y. Pontikes, Rheology of an alkali-activated fe-rich slag suspension: identifying the impact of the activator chemistry and slag particle interactions, J. Non-Cryst. Solids 561 (2021), 120747, https://doi.org/10.1016/j.jnoncrysol.2021.120747.
[31] G. Beersaerts, G. Ascensão, Y. Pontikes, Modifying the pore size distribution in fe-rich inorganic polymer mortars: an effective shrinkage mitigation strategy, Cem. Concr. Res. 141 (2021), 106330, https://doi.org/10.1016/j.cemconres.2020.106330.
[32] N.M. Piatak, M.B. Parsons, R.R. Seal II, Characteristics and environmental aspects of slag: a review, Appl. Geochem. 57 (2015) 236–266, https://doi.org/10.1016/j.apgeochem.2014.04.009.
[33] A. Adediran, J. Yliniemi, M. Illikainen, Fayalite slag as binder and aggregate in alkali-activated materials—interfacial transition zone study, Proceedings 34 (2019) 1, https://doi.org/10.3390/proceedings2019034001.
[34] K. Komnitsas, L. Yurramendi, G. Bartzas, V. Karmali, E. Petrakis, Factors affecting co-valorization of fayalitic and ferronickel slags for the production of alkali activated materials, Sci. Total Environ. 721 (2020), 137753, https://doi.org/10.1016/j.scitotenv.2020.137753.
[35] A. Nikolov, Alkali-activated geopolymers based on iron-rich slag from copper industry, IOP Conf. Ser.: Mater. Sci. Eng. 951 (2020), 012006, https://doi.org/10.1088/1757-899X/951/1/012006.
[36] SFS-EN 196-1, Methods of Testing Cement. Part 1: Determination of Strength, 2011.
[37] EN 1015-3, Methods of test for mortar for masonry. Determination of consistence of fresh mortar (by flow table), in: European Committee for Standardization 1999, 1999.
[38] ASTM C 666/C 666M – 03, Standard Test Method for Resistance of Concrete to Rapid Freezing and Thawing, 2008.
[39] T. Luukkonen, Z. Abdollahnejad, J. Yliniemi, M. Mastali, P. Kinnunen, M. Illikainen, Alkali-activated soapstone waste - mechanical properties, durability, and economic prospects, Sustain. Mater. Technol. 22 (2019), https://doi.org/10.1016/j.susmat.2019.e00118.
[40] H. Nguyen, P. Kinnunen, V. Carvelli, M. Illikainen, Durability of ettringite-based composite reinforced with polypropylene fibers under combined chemical and

physical attack, Cem. Concr. Compos. 102 (2019) 157–168, https://doi.org/10.1016/j.cemconcomp.2019.04.021.
[41] M. Mastali, P. Kinnunen, A. Dalvand, R. Mohammadi Firouz, M. Illikainen, Drying shrinkage in alkali-activated binders – a critical review, Constr. Build. Mater. 190 (2018) 533–550, https://doi.org/10.1016/j.conbuildmat.2018.09.125.
[42] J. Singh, S.P. Singh, Evaluating the alkali-silica reaction in alkali-activated copper slag mortars, Constr. Build. Mater. 253 (2020), 119189, https://doi.org/10.1016/j.conbuildmat.2020.119189.
[43] G. Beersaerts, G. Ascensão, Y. Pontikes, Modifying the pore size distribution in fe-rich inorganic polymer mortars: an effective shrinkage mitigation strategy, Cem. Concr. Res. 141 (2021), 106330, https://doi.org/10.1016/j.cemconres.2020.106330.
[44] J.N. Yankwa Djobo, A. Elimbi, H. Kouamo Tchakouté, S. Kumar, Mechanical properties and durability of volcanic ash based geopolymer mortars, Constr. Build. Mater. 124 (2016) 606–614, https://doi.org/10.1016/j.conbuildmat.2016.07.141.
[45] F. Pacheco-Torgal, Z. Abdollahnejad, A.F. Camões, M. Jamshidi, Y. Ding, Durability of alkali-activated binders: a clear advantage over Portland cement or an unproven issue? Constr. Build. Mater. 30 (2012) 400–405, https://doi.org/10.1016/j.conbuildmat.2011.12.017.
[46] V. Sata, A. Sathonsaowaphak, P. Chindaprasirt, Resistance of lignite bottom ash geopolymer mortar to sulfate and sulfuric acid attack, Cem. Concr. Compos. 34 (2012) 700–708, https://doi.org/10.1016/j.cemconcomp.2012.01.010.
[47] J.C. Kuri, P.K. Sarker, F.U.A. Shaikh, Sulphuric acid resistance of ground ferronickel slag blended fly ash geopolymer mortar, Constr. Build. Mater. 313 (2021), 125505, https://doi.org/10.1016/j.conbuildmat.2021.125505.
[48] B. EN, 1-1: 2004+ A1: 2014 Eurocode 2: Design of Concrete Structures—General Rules and Rules for Buildings, BS EN. 12871 (1992), 2013.
[49] ASTM C62, ASTM C62-99: Standard Specification for Building Brick (Solid Masonry Units Made From Clay or Shale), 1999.
[50] A. Mohsen, H.A. Abdel-Gawwad, M. Ramadan, Performance, radiation shielding, and anti-fungal activity of alkali-activated slag individually modified with zinc oxide and zinc ferrite nano-particles, Constr. Build. Mater. 257 (2020), 119584, https://doi.org/10.1016/j.conbuildmat.2020.119584.
[51] O.S.B. Al-Amoudi, M. Maslehuddin, Y.A.B. Abdul-Al, Role of chloride ions on expansion and strength reduction in plain and blended cements in sulfate environments, Constr. Build. Mater. 9 (1995) 25–33, https://doi.org/10.1016/0950-0618(95)92857-D.
[52] J. Singh, S. Singh, Development of alkali-activated cementitious material using copper slag, Constr. Build. Mater. 211 (2019) 73–79, https://doi.org/10.1016/j.conbuildmat.2019.03.233.
[53] J.L. Provis, S.A. Bernal, Geopolymers and related alkali-activated materials, Annu. Rev. Mater. Res. 44 (2014) 299–327, https://doi.org/10.1146/annurev-matsci-070813-113515.
[54] A. Peys, C.E. White, H. Rahier, B. Blanpain, Y. Pontikes, Alkali-activation of CaO-FeOx-SiO2 slag: formation mechanism from in-situ X-ray total scattering, Cem. Concr. Res. 122 (2019) 179–188, https://doi.org/10.1016/j.cemconres.2019.04.019.
[55] S.A. Bernal, J.L. Provis, B. Walkley, R.San Nicolas, J.D. Gehman, D.G. Brice, A. R. Kilcullen, P. Duxson, J.S.J. van Deventer, Gel nanostructure in alkali-activated binders based on slag and fly ash, and effects of accelerated carbonation, Cem. Concr. Res. 53 (2013) 127–144, https://doi.org/10.1016/j.cemconres.2013.06.007.
[56] P.N. Lemougna, A. Nzeukou, B. Aziwo, A.B. Tchamba, K. Wang, U.C. Melo, X. Cui, Effect of slag on the improvement of setting time and compressive strength of low reactive volcanic ash geopolymers synthetized at room temperature, Mater. Chem. Phys. (2019), 122077, https://doi.org/10.1016/j.matchemphys.2019.122077.